Effect of recycled tyre polymer fibre on engineering properties of sustainable strain hardening geopolymer composites

Hui Zhong, Mingzhong Zhang*

Department of Civil, Environmental and Geomatic Engineering, University College London, London, WC1E 6BT, UK

Abstract: Strain hardening geopolymer composite (SHGC) processing superior tensile ductility and multiple cracking is a promising alternative to traditional ductile cementitious composites whereas the extremely high cost of polyvinyl alcohol (PVA) fibres limits its large-scale application. This paper presents a feasibility study of replacing PVA fibres with recycled tyre polymer (RTP) fibres to reduce the material cost of fly ash-slag based SHGC and ease the pressure on environmental impact induced by the vast amount of waste tyres, focusing on the influences of PVA fibre content (1.0-2.0% by volume) and RTP fibre replacement dosage (0.25-1.0% by volume) on the engineering properties especially uniaxial tensile behaviour, microstructure, material cost and environmental impact. Results indicate that the incorporation of RTP fibres into SHGC can lessen the loss in flowability and compressive strength due to the addition of PVA fibres. The drying shrinkage of SHGC containing RTP fibres is effectively reduced by about 35.69% and 17.33% as compared with the plain matrix and SHGC containing 2.0% PVA fibre, respectively. Although the presence of more RTP fibres diminishes the uniaxial tensile behaviour of SHGC, the cost and embodied energy of SHGC utilising RTP fibres are reduced by up to 34.52% and 16.23%, respectively. SHGC with 1.75% PVA fibre and 0.25% RTP fibre can be considered as the optimal mixture as it provides adequate engineering properties including a tensile strain capacity of around 2.5%, lower material cost and lower environmental impact compared to the typical SHGC with 2.0% PVA fibre.

Keywords: Engineered geopolymer composites; Fibre reinforced concrete; Strain hardening behaviour; Micromechanics; Sustainability assessment

1. Introduction

Conventional concrete is strong in compression but exhibits brittle failure under tension with a tensile strain capacity of only 0.01% [1], which would considerably impair the long-term behaviour of concrete structures even when steel reinforcement is incorporated [2]. To mitigate these concerns, strain hardening cementitious composite (SHCC) is developed in the early 1990s [1], which is a broad class of fibre reinforced concrete featuring strain hardening and multiple cracking under tension [3-5]. The main difference between SHCC and normal concrete or fibre reinforced concrete under tensile loading is that the tensile stress of SHCC continues to rise or remains steady with the increase of tensile strain after the initiation of the first crack, achieving superior tensile ductility. Typically,

* Corresponding author. E-mail address: mingzhong.zhang@ucl.ac.uk (M. Zhang)

SHCC processes a tensile strain capacity over 2% and a crack width below 100 μm under the loading state [5, 6]. However, SHCC requires a higher dosage of Portland cement resulting in higher material cost as well as lower greenness [7]. Owing to the increasing production of Portland cement, the cement industry is responsible for about 8% of the global emitted CO_2 [8], and the CO_2 emission and energy consumption from the cement manufacture would be expected to increase by around 85-105 Gt and about 420-505 TJ by the year of 2050 [9]. Thus, it is vital to seek for a sustainable alternative binder material for SHCC.

Strain hardening geopolymer composite (SHGC) with higher greenness is considered as a promising substitute to SHCC. As the binder of SHGC, geopolymer (also called alkali-activated material) is an inorganic polymer synthesised through the alkali-activation of industrial by-products such as fly ash (FA) that is the most commonly used one. For instance, Ohno and Li [10] conducted a feasibility study of FA-based SHGC using two different kinds of FA and developed a FA-based SHGC with a tensile strain of up to 4.5%. Besides, they proposed an innovative design method of FA-based SHGC which integrates design of experiment, micromechanical modelling, and material sustainability indices [11]. Nematollahi et al. [12, 13] studied the effect of four different types of activators on the fresh and mechanical properties of FA-based SHGC and found that the SHGC activated by a combination of sodium hydroxide (SH) and sodium silicate (SS) solutions can exhibit better material behaviour, especially under tensile and flexural loadings. In addition, Nematollahi et al. [14] observed that the incorporation of excessive fine sand or the utilisation of coarse sand adversely influenced the strain hardening behaviour of the composites. Farooq et al. [15] explored the tensile performance of FA-based SHGC reinforced with various micro-fibres and concluded that all mixtures reinforced with polyvinyl alcohol (PVA) fibres can present a clear strain hardening feature with a tensile strain of higher than 0.52%. However, FA-based SHGC requires elevated curing temperature to gain strength, where this curing regime is not suitable for cast-in-situ application [16]. Although several studies [17-20] showed that SHGC utilising ground granulated blast-furnace slag (GGBS) can attain a superior tensile ductility (up to 7.5%), the SHGC incorporating solely GGBS has poor workability, low setting time and high shrinkage strain [21-23] that are not favourable for the engineering applications.

Thus, an increasing number of studies have attempted to combine GGBS with FA to produce SHGC not only to address the above concerns but also to improve the overall engineering properties [16, 24-27]. Nematollahi et al. [16] developed a FA-GGBS based one-part SHGC under either ambient temperature curing or heat curing, which can exhibit a tensile strength of 4.4-4.6 MPa and a tensile strain of 3.6-4.2%, respectively. Furthermore, Nematollahi et al. [24] examined the feasibility of using polyethylene (PE) fibres in FA-GGBS based one-part SHGC, who found that a tensile strain of about 4.9% can be obtained for this type of SHGC under ambient temperature curing. Ling et al.

[25] studied the effect of FA/GGBS ratio on the mechanical properties of SHGC and revealed that incorporating a lower content of GGBS (20% by weight) can increase the strength properties of SHGC while maintaining the strain hardening feature. Zhang et al. [26] explored the influence of silicate modulus of activator (0.8-1.5) on the tensile behaviour of FA-GGBS based SHGC and suggested that 1.2 can be considered as the optimal silica modulus for the sodium-based activator. Wang et al. [27] found that the incorporation of fine sand up to 20% (by weight of binder) can improve the flexural behaviour of FA-GGBS based SHGC compared to that without sand. Although replacing Portland cement with a geopolymer binder can reduce the carbon footprint and environmental impact, the costs of commonly used PVA and PE fibres hinder the large-scale application of SHGC. For a typical M45 SHCC, the cost of PVA fibres accounts for about 80% of the total material cost [28]. Moreover, the cost of PE fibres is even higher than that of PVA fibres (about 5-8 times) [29, 30]. Apart from the economic aspect, the increasing manufacture of virgin synthetic fibres may consume more non-renewable natural resources and generate more wastes [31], implying that the increasing application of SHGC reinforced with PVA fibres or PE fibres would impede the sustainable development of the construction industry. As a result, to improve the cost-effectiveness of SHGC while reducing the environmental impacts associated with the virgin fibres, one possible solution is to replace the commonly used virgin fibres with recycled fibres [31, 32].

Until now, extremely limited studies have been reported on using recycled fibres to replace virgin PVA or PE fibres in either SHCC or SHGC. In SHCC, recycled polyethylene terephthalate (PET) fibres have been mainly used to replace virgin PVA fibres. Choi et al. [33] and Yu et al. [34] reported that the tensile behaviour of SHCC with recycled PET fibres was diminished in comparison with SHCC containing 2.0% (by volume) PVA fibre. However, acceptable tensile properties could be still achieved for certain practical applications when a proper dosage of recycled PET fibre is incorporated (up to 1.0%). Besides, it is worth noting that the material cost and embodied energy of SHCC can be considerably decreased after the replacement of PVA fibres with recycled PET fibres. Lu et al. [35] observed that the utilisation of recycled PET fibres can improve the impact resistance of SHCC. Apart from recycled synthetic fibres, recycled tyre steel (RTS) fibres extracted from end-of-life tyres were used to replace PVA fibres in SHCC to optimise its mechanical properties and reduce its material cost [36]. It was stated that combining 1.5% PVA fibre and 0.5% RTS fibre in SHCC can achieve the optimal engineering properties [36]. Regarding the usage of recycled fibres to replace PVA fibres in SHGC, only one relevant study [37] can be found, which investigated the effect of RTS fibres on the engineering properties of SHGC and noted that RTS fibres are favourable for the improvements of drying shrinkage resistance and compressive strength although the flexural strength is weakened after the incorporation of RTS fibres. It is worth mentioning that besides the above-mentioned benefits, incorporating RTS fibres in SHCC or SHGC can also significantly enhance the sustainability of the

composites. It was reported that approximately 1500 million end-of-life tyres are created yearly [38], where the enormous amount of these waste tyres would induce several environmental problems and increase the burden on landfilled areas [39]. Recycling these waste tyres as shredded materials is an effective approach to mitigate the above issues and RTS fibre is the major output of the recycling process. Thus, successful applications of RTS fibres in the construction industry can greatly enhance its sustainability by reducing the environmental impact. In addition, recently, a growing emphasis has been placed on the use of another recycled tyre material, recycled tyre polymer (RTP) fibre, in cementitious material as fibre reinforcement. The motivation of introducing RTP fibres in the construction industry is to find a possible usage for them, as storing RTP fibres is a big challenge that may lead to several environmental problems [40]. The existing studies on the effect of RTP fibres in cementitious composites found that the presence of RTP fibres can improve the resistance of the resultant composites to fire spalling [41], autogenous, plastic and drying shrinkage cracking [42-44], and freeze-thaw cycles [40, 45], and enhance their dynamic properties and fatigue behaviour [46-48]. Although RTP fibres in cementitious composites have several positive impacts, the feasibility of using RTP fibres in geopolymer has not been extensively studied, which would limit the widespread application of RTP fibres. From the economic and environmental perspectives, it is promising to develop a cost-effective and sustainable SHGC with acceptable engineering properties through the replacement of commonly used PVA fibres with RTP fibres. To verify this hypothesis, it is vital to explore the effect of RTP fibres on the engineering properties and sustainability of FA-GGBS based SHGC, which has not been addressed.

The main purpose of this work is to investigate the feasibility of partially replacing PVA fibres with RTP fibres to produce sustainable SHGC with acceptable engineering properties. Firstly, a series of tests were carried out to study the influences of PVA fibre dosage (1.0%, 1.5% and 2.0% by volume) and RTP fibre replacement of PVA fibres (0.25%, 0.5%, 0.75% and 1.0% by volume) on the engineering properties of FA-GGBS based SHGC including flowability, drying shrinkage, compressive strength and uniaxial tensile behaviour. Special focus was placed on the uniaxial tensile behaviour of SHGC in terms of stress-strain response, tensile strength, tensile strain capacity, strain energy and fracture pattern as well as the micromechanical analysis in terms of stress-crack opening behaviour and strain hardening indices. Then, the fibre failure condition after the uniaxial tensile test was characterised using scanning electron microscopy (SEM) to get a comprehensive understanding of tensile behaviour and fracture mechanism of SHGC. Afterwards, the economic viability and sustainability of all mixtures in terms of material cost and life cycle inventory data were assessed and discussed. Finally, an optimal mixture of SHGC was proposed considering the material cost, environmental impact, and acceptable engineering properties.

2. Experimental program

2.1. Raw materials

Low calcium FA as per ASTM C618-17a [49] and GGBS with a hydration modulus (i.e. the ratio of CaO + MgO + Al_2O_3 to SiO_2) of 2.0 were used as binder materials in this study, the chemical composition of which is given in Table 1. It is worth noting that the hydration modulus of GGBS should be higher than 1.4 to ensure good hydration characteristics [50]. Fig. 1a presents the particle size distribution of FA and GGBS, where the corresponding average particle sizes are summarised in Table 1. As shown in Fig. 1b and c, the shape of FA particles is spherical while GGBS particles are mostly angular. It was found that the fracture toughness of the cementitious matrix increases with the size of aggregate [51], which may impair the strain hardening behaviour of composites. To control the fracture toughness of the geopolymer matrix, fine silica sand (see Fig. 1a and d) with a maximum particle size of 250 µm and a mean particle size of 130 µm was utilised as fine aggregate. 10 M SH solution and SS solution with a silicate modulus (SiO_2/Na_2O ratio) of 3.15 (Na_2O: 8.5 wt%, SiO_2: 26.8 wt%, H_2O: 64.7 wt%) were used as alkaline activator (AL). To enhance the workability of mixtures, a modified polycarboxylate-based superplasticiser (SP) (Sika®ViscoFlow®3000) was applied. Table 2 lists the specific gravity of these raw materials.

PVA fibres (Kuraray Co., Ltd., Japan) and RTP fibres obtained mainly from the truck tyres were used as fibre reinforcements in this study. Since many rubber particles attach the RTP fibres, a sieving/cleaning process based on a previous study [40] proceeded on the as-received RTP fibres before usage. The detailed sieving/cleaning method was reported in [47]. Fig. 2 illustrates the physical appearance of PVA and RTP fibres (after processed) using various image-capturing instruments including digital camera, digital microscope, SEM equipment. It is worth noting that the brightness of fibres shown in Fig. 2c and d is relatively higher due to the large exposure level used during the image capturing procedure. Given that RTP fibres may contain different organic compositions, attenuated total reflectance Fourier transform infrared spectroscopy (ATR-FTIR) was applied as it is considered as a fast, suitable, non-destructive and inexpensive method for fibre identification [52]. As previous studies [42, 46] found that the primary composition of RTP fibres is PET, the ATR-FTIR method was applied on both RTP and PET fibres using a Nicolet iS10 FT-IR spectrometer with an ATR accessory as per ASTM E1252-98 [53] to investigate the primary composition of RTP fibres. Fig. 3 presents the FTIR spectra of RTP and PET fibres, indicating that the spectrum of RTP fibre mostly matched that of PET fibre considering various characteristic peak positions within a range of wavenumber. The main peaks [54-58] for PET fibre were highlighted and marked in Fig. 3. For instance, the peak at 2968.51 cm^{-1} was related to the stretching vibration of methylene group ($-CH_2$) while the significant peak at 1713.17 cm^{-1} can be attributed to the stretching vibration of carbonyl group (C=O). Besides, the peak at 722.92 cm^{-1} was corresponding to the out-of-plane bending

vibration of the CH on benzene ring. As shown in Fig. 3, compared to PET fibre, the spectrum of RTP fibre presented similar peaks at 2917.85, 1712.89, 1245.26, 1096.69, 1018.30 and 722.56 cm^{-1}, suggesting that the RTP fibres used in this study are mainly composed of PET. As seen in Fig. 2, the RTP fibres are not uniform in dimension. Thus, a group of RTP fibre samples were characterised in terms of length and diameter using a digital microscope and a fibre diameter tester (XGD-1 Fibre Diameter Tester), respectively. Fig. 4 illustrates the distribution of length (in mm) and diameter (in μm) of RTP fibres. It can be found that around 86.67% of RTP fibres are shorter than 8 mm and 82.67% of them have a diameter of less than 26 μm. Besides, the elongation, tensile strength, and elastic modulus of RTP fibres were measured using a fibre tensile tester (XQ-1A Fibre Tensile Tester). The density of RTP fibres was measured using a gas displacement pycnometry system (AccuPyc II 1345, USA), where helium was used as the displacement medium. During the sieving/cleaning process of as-received RTP fibres, the percentages of RTP fibres and rubber particles (attached with very short RTP fibres) were determined, which were 39.81% and 60.19%, respectively. Table 3 presents the main properties of PVA and RTP fibres.

2.2. Mix proportions

Table 4 lists the mix proportions investigated in this study. Regarding the geopolymer matrix, the mass ratios of FA/GGBS, silica sand/binder, AL/binder, the molarity of SH solution, and SS/SH were selected as 4.0, 0.2, 0.45, 10 M, and 1.5 based on previous studies [25, 27, 59]. The mass ratio of SP/binder was set as 0.01 as it was reported that adding this content of SP can significantly enhance the workability of FA-GGBS based geopolymer paste [60]. These parameters were kept constant and the changing parameters were fibre type and dosage. For the meaning of mixture label given in Table 4, for instance, P1.75R0.25 denotes the geopolymer matrix reinforced with two types of fibres, where ‘P1.75’ stands for the dosage of PVA fibre (1.75% by volume) while ‘R0.25’ represents the dosage of RTP fibre (0.25% by volume). P0R0 is the reference mixture (no fibre addition). P1.0R0, P1.5R0 and P2.0R0 were designed to investigate the influence of PVA fibre dosage on the engineering properties of SHGC. These mixtures were also considered as references. P1.75R0.25, P1.5R0.5, P1.25R0.75 and P1.0R1.0 were designed and compared with P2.0R0 to explore the effect of RTP fibre replacement on the engineering properties of SHGC. The upper limit of RTP fibre replacement content was set as 1.0% considering that: (1) it would be difficult for SHGC to exhibit strain hardening behaviour when the content of PVA fibres is less than 1.0% [61]; (2) the addition of RTP fibres over 1.0% may dramatically weaken the hardened properties of the composites [46]. P1.5R0.5 and P1.0R1.0 were compared with P1.5R0 and P1.0R0, respectively, to estimate the effect of RTP fibre addition on the engineering properties of PVA fibre reinforced SHGC.

2.3. Sample preparation

Regarding the sample preparation, the SH solution was prepared by mixing SH pellets (>99% purity) with tap water, 24 h prior to the mixing process. Herein, 400 g of SH pellets were dissolved in the tap water to prepare 1 L of 10 M SH solution. All mixtures shown in Table 4 were prepared using a 20 L planetary mixer with a constant mixing speed of 140 rpm. Firstly, FA, GGBS and silica sand were dry mixed for 90 s followed by the gradual addition of AL. Then, the mixing was continued for another 180 s before the addition of SP. Once a consistent mixture was obtained, the PVA fibres were slowly added. It should be mentioned that for the mixtures containing both PVA and RTP fibres, the RTP fibres were first mixed with a certain content of AL to avoid fibre clumping or balling [43, 44]. The mixing process finished when the fibres were uniformly distributed in the mixtures. The total mixing time of all mixtures (except plain matrix mixture) was approximately 10 min. A proportion of the fresh mixtures was used for the fresh property test while the remaining was cast in various moulds with sufficient vibration. The samples were sealed by the plastic sheet at ambient temperature (20 ± 2 °C) to avoid moisture loss. After 24 h, the samples (except samples for drying shrinkage test) were de-moulded and cured in a standard curing room (20 ± 2 °C, 95% RH) until desired testing ages.

2.4. Test methods

Table 5 presents the overall testing scheme of this study including the number of specimens and complied standard for each test. The methodology of each test will be described in detail below.

2.4.1. Flow table test

According to ASTM C1437-15 [62], the flow table test was conducted to assess the flowability of fresh mixtures. Firstly, the fresh mixture was poured into a truncated conical mould with a height of 50 mm, a top diameter of 70 mm and a bottom diameter of 100 mm. The spread diameter of each fresh mixture was measured after two steps: (1) lifting the truncated conical mould; (2) tapping the flow table 25 times. For each mixture, three repeated tests were conducted.

2.4.2. Drying shrinkage test

The drying shrinkage test was performed on the 25 mm × 25 mm × 280 mm prismatic specimen with a gauge length of 250 mm. Upon the de-moulding of the specimen, the initial comparator reading of the specimen was taken immediately. Subsequently, the specimen was cured under an environment with a temperature of 20 ± 2 °C and relative humidity of 50% ± 5%. The comparator readings at various curing ages were recorded. The drying shrinkage was determined by comparing the subsequent comparator readings with the initial comparator reading based on ASTM C490-17 [63].

2.4.3. Compression test

The compression test was conducted on the 50 mm × 50 mm × 50 mm cubic specimen at 28 d in accordance with ASTM C109/C109M-20b [64]. The loading speed of the compression testing machine was kept fixed for all mixtures as 0.3 MPa/s.

2.4.4. Uniaxial direct tension test

The uniaxial direct tension test was carried out on the dog-bone shaped specimen at 28 d according to the recommendation of Japan Society of Civil Engineers (JSCE) [65]. Fig. 5 shows the schematic illustration of the experimental setup and the dimension of the dog-bone shaped specimen. As seen in Fig. 5a, the dog-bone shaped specimen was loaded uniaxially with a loading rate of 0.5 mm/min and two linear variable displacement transducers (LVDTs) were installed to measure the tensile deformation at both sides of the specimen within a gauge length of 80 mm. Besides, the region of the gauge length was used for the crack analysis (Fig. 5b). Regarding the crack analysis, the residual crack number and crack width of each specimen were determined using a digital microscope (WM401WIFI, Shanghai) until the load removal. Although the residual crack width could not fully represent the crack width whilst the tensile loading of the specimen, the result can still be used to evaluate the effect of fibres on the crack-controlling ability of the composite. Besides, the fibre failure status across the fracture surface was captured using a digital microscope.

2.4.5. Micromechanical and microstructural investigation

SHCC with high tensile ductility and multiple cracking can be designed and tailored based on the micromechanics theory [1, 5, 66], through the optimisation of synergistic interactions between microstructural components. According to the micromechanical design theory [1], two criteria (strength-based and energy-based) need to be satisfied to achieve strain hardening and multiple cracking behaviour for the composite. Fig. 6 presents a typical tensile stress-crack opening curve for the fibre bridging of SHCC, which will be used to explain how the two criteria can be fulfilled [1].

Regarding the strength-based criterion, the following condition must be satisfied for the crack initiation:

$$\sigma_{fc}, \sigma_c < \sigma_0 \quad (1)$$

where σ_{fc} is the stress required to initiate the first crack, σ_c is the stress required to form another crack (multiple cracks are formed already), and σ_0 is the fibre bridging stress.

Eq. (1) suggests that the capacity of bridging fibres must be higher than the tensile stresses needed to initiate the first crack and a new crack. When the first crack is initiated, the crack propagation mode of the composite is dependent on the bridging fibres [29]. It is worth mentioning that the crack propagation modes of SHCC and SHGC differ considerably from the Griffith crack propagation mode that is normally observed in ordinary fibre reinforced cementitious composites [1]. In Griffith crack propagation mode, the crack opening increases indefinitely with crack length while the applied load must be decreased to ensure the equilibrium during the growth of the crack. On the contrary, flat crack propagation mode is typically observed in both SHCC and SHGC, in which the applied load and the crack opening are kept as constant as the crack length extends indefinitely [1, 67]. Thus, the following energy-based criterion needs to be fulfilled for the flat crack propagation:

$$J'_b > J_{tip} = \sigma_{ss}\delta_{ss} - \int_0^{\delta_{ss}} \sigma(\delta)\, d\delta = K_m^2/E_m \quad (2)$$

$$\sigma_0\delta_0 - \int_0^{\delta_0} \sigma(\delta)\, d\delta = J'_b \quad (3)$$

where J'_b is the maximum complementary energy, J_{tip} is the crack tip toughness, δ_0 is the crack opening corresponding to the maximum fibre bridging stress (σ_0), δ_{ss} is the crack opening corresponding to the steady-state bridging stress (σ_{ss}), E_m is the elastic modulus of the matrix, and K_m is the fracture toughness of the matrix.

Thus, it is important to evaluate whether the studied mixtures (Table 4) can meet the above criteria. In this study, two important indices, i.e., σ_0/σ_{fc} and J'_b/J_{tip}, were experimentally determined using a series of tests. The single crack direct tension was carried out to attain the tensile stress-crack opening curve of the composite (Fig. 6) at 28 d and then to determine σ_0 and δ_0. A schematic illustration of the experimental configuration is given in Fig. 7. The dimension of the tested specimen here was the same as that used in the uniaxial direct tension test (see Section 2.4.4) while notches were cut around the mid-height of the specimen. The dimensions of the notched area and the remained area are given in Fig. 7. The loading rate of the test was kept constant at 0.5 mm/min. Two LVDTs were mounted to measure the crack opening of the single crack. Through conducting the uniaxial direct tension test on the matrix mixture (P0R0) at 28 d, two parameters, σ_{fc} and E_m, were subsequently evaluated. To obtain K_m, three-point bending test was performed on the 40 mm × 40 mm × 160 mm prismatic specimen with a notch at 28 d under a constant loading rate of 1 mm/min according to RILEM FMC-50 [68], the experimental configuration of which is presented in Fig. 8. The thickness, length and depth of the single notch were 1.0, 40 and 12 mm, respectively. K_m can be calculated by [69]:

$$K_m = \frac{1.5\left(F_p + \frac{mg}{2} \times 10^{-2}\right) \times 10^{-3} \times S \times a_0^{\frac{1}{2}}}{th^2} f(a) \quad (4)$$

$$f(a) = \frac{1.99 - a(1-a)(2.15 - 3.99a + 2.7a^2)}{(1+2a)(1-a)^{3/2}} \quad (5)$$

$$a = \frac{a_0}{h} \quad (6)$$

where F_p is the peak load recorded during the three-point bending test, m is the mass of the tested specimen, S is the loading span, a_0 is the depth of the notch, t is the thickness of the tested specimen, and h is the height of the tested specimen.

For the microstructural characterisation, several pieces of samples were obtained from the fracture surface of the specimen after uniaxial tensile test and then characterised using SEM equipment (FEI, QUANTA FEG 250, USA). The objective was to explore the surface condition and failure mode of the fibres, which are important to the understanding of the fracture mechanism of SHGC. Regarding the SEM test, the acceleration voltage was set as 20 kV while the working distance was around 10 mm.

3. Results and discussion

3.1. Flowability

Fig. 9a shows the spread diameters of all mixtures, which can reflect the workability of fresh mixtures. The mixture without any fibre reinforcement (P0R0) had the highest spread diameter of around 250 mm (Fig. 9b) while regardless of fibre type and dosage, the spread diameters of SHGC became lower when the fibres were incorporated, which can be mainly attributed to the contact network between the fibres inside the geopolymer matrix [70]. Thus, the movement of the fresh mixture is restricted, resulting in an increase in overall yield stress. Regarding the effect of PVA fibres, the reduction in spread diameter caused by the addition of 1.0% PVA fibre was limited, only 7.28% lower in comparison with P0R0. Nevertheless, the higher dosages of PVA fibre (1.5% and 2.0%) reduced the spread diameter of SHGC by 18.62-22.10%, which is in agreement with previous studies on FA-based [15] and FA-GGBS based [37] SHGC. There exists a critical fibre dosage, where fibre clumping or balling tends to occur when the incorporated fibre dosage exceeds it [70]. It is suggested that the critical fibre dosage is affected by the fibre aspect ratio and varies between different fibres, ranging from 0.2-2.0% (by volume) for geopolymer and cementitious composites [71, 72]. In this study, the critical fibre dosage of PVA fibres is likely in the interval between 1.0% and 1.5%.

Fig. 9a indicates a slight decrease of 12.22% in spread diameter when 0.5% RTP fibre was added to the mono-PVA fibre reinforced SHGC (P1.5R0), while the presence of 1.0% RTP fibre in SHGC resulted in a more obvious loss in spread diameter. As mentioned in Section 2.3, part of the AL was used to mix with RTP fibres during the sample preparation, which may reduce the liquid content inside the mixture, leading to an increase of viscosity. Considering the effect of RTP fibres, replacing 0.25% PVA fibre with RTP fibre in SHGC exhibited slightly better workability (Fig. 9a), implying that a small dosage of RTP fibres would not considerably influence the workability of the composites. This could be ascribed to the smaller aspect ratio of RTP fibres [72]. However, the spread diameters of SHGC containing RTP fibres higher than 0.25% were 8.31-11.91% smaller than that of P2.0R0, revealing that the critical fibre dosage of RTP fibres may fall in the range of 0.25-0.5%. This needs to be further verified by investigating the mono-RTP fibre reinforced geopolymers with various RTP fibre dosages. Furthermore, as PVA fibres are stiffer than RTP fibres, combining PVA fibres with a larger content of RTP fibres (over 0.25%) would result in a congested fibre network. Therefore, the

flowable geopolymer matrix may be difficult to pass through this network properly [70], affecting the workability of SHGC adversely. As shown in Fig. 9a, P1.0R1.0 exhibited the lowest spread diameter of about 171 mm, and thus more vibration would be required for this mixture to increase its compactness inside the mould to avoid a conspicuous loss of hardened properties (Fig. 9c). It should be noted that no pronounced fibre clumping or balling was observed for all SHGC mixtures during the sample preparation.

3.2. Drying shrinkage

Due to the high dosage of cement and low volume fraction of fine aggregate, SHCC typically exhibits a very high drying shrinkage, which can promote the initiation of early-age cracking and thereby weakening the long-term durability of concrete structures [73]. It was found that geopolymer matrix generally presents higher shrinkage than cementitious matrix, which is dependent on binder type and AL characteristics [74], suggesting that SHGC may pose a larger restraint to the enhancement of durability than SHCC although fibres are incorporated.

Fig. 10 depicts the drying shrinkage of all mixtures up to 28 d. It can be observed that the drying shrinkage of all mixtures developed rapidly up to 7 d, after which the development of drying shrinkage gradually slowed down. Increasing the PVA fibre dosage consistently decreased the drying shrinkage of SHGC, where the 28-d drying shrinkage strains of P1.0R0, P1.5R0 and P2.0R0 were 11.29%, 21.06% and 22.22% respectively lower than that of P0R0. It is noticed that P1.5R0 and P2.0R0 presented a comparable performance in restraining the drying shrinkage of SHGC, which is inconsistent with the findings reported in previous studies on geopolymer composites [70]. As mentioned in Section 3.1, exceeding the critical fibre dosage may entrap more air during the mixing, which would result in a higher internal porosity around the fibres. Therefore, the internal moisture inside SHGC can move more easily through the formed pore network, impairing the shrinkage resistance [75].

As seen in Fig. 10, the presence of 0.5% and 1.0% RTP fibre in SHGC improved the shrinkage resistance at different extents, where a reduction of 27.51% in drying shrinkage can be observed after incorporating 1.0% RTP fibre into P1.0R0. Excellent shrinkage-restraining behaviour was also reported for cementitious composites containing RTP fibres [40, 42, 44], which can be attributed to the release of temporarily blocked liquid content at the surfaces of RTP fibres and attached rubber particles [42]. On the other hand, as shown in Fig. 10, the drying shrinkage strain of P2.0R0 was approximately 11671 με, which was much higher than that of traditional SHCC (1200 με) [73], confirming the higher drying shrinkage in SHGC. However, it is interesting to note that the increase of RTP fibre replacement ratio resulted in a general decreasing trend in drying shrinkage, where the reduction was more pronounced when 0.75% or 1.0% PVA fibre was replaced with RTP fibre. P1.25R0.75 and P1.0R1.0 presented a drying shrinkage of around 10751 με and 9649 με at 28 d,

which is 7.88% and 17.33% lower than that of P2.0R0, respectively. As mentioned earlier, the released liquid content from the surfaces of RTP fibres can partially contribute to the reduction in drying shrinkage while the synergistic effect between PVA fibres and RTP fibres is also beneficial to restrain the drying shrinkage via the crack-controlling at two scales. As shown in Table 3, PVA fibres have relatively a longer length which helps limit the propagation of macro-cracks while micro-cracks or tiny internal flaws can be bridged and restrained by the RTP fibres with relatively shorter lengths. Therefore, the shrinkage stress across the cracks can be transferred to the bridging fibres, minimising the overall shrinkage strain. Although the presence of RTP fibres can help reduce the drying shrinkage of SHGC, the 28-d drying shrinkage of P1.0R1.0 is still higher than that of conventional SHCC, which may hinder the engineering application of SHGC, e.g. as a repair material to bond with the concrete possessing very low shrinkage [76]. To further reduce the drying shrinkage of SHGC, several possible approaches can be applied such as incorporating shrinkage-reducing admixture [77, 78] and increasing the sand content [27].

3.3. Compressive strength

The presence of fibres can simultaneously exert both positive and negative impacts on the compressive strength of cementitious composites, which are associated with the fibre type and fibre properties, especially stiffness [70, 79]. The compressive strength of all mixtures at 28 d is illustrated in Fig. 11a. The compressive strength of SHGC containing mono-PVA fibres presented a decreasing trend. In comparison with P0R0, the addition of 1.5% and 2.0% PVA fibre led to a reduction of 14.49% and 24.94%, respectively, suggesting that the negative influence caused by the addition of PVA fibres on compressive strength suppressed its positive influence. Regarding the negative influence, the composite has a higher tendency to entrap more air during the mixing after exceeding the critical fibre dosage, which may in turn decrease the compactness of the whole composite, as discussed in Section 3.1. Therefore, local fractures tend to occur around the fibres and ultimately weaken the composite's compressive strength [70]. The reduced compressive strength of SHCC caused by the fibre incorporation become more obvious with the reducing water-to-binder (w/b) ratio, as reported by Yu et al. [79] who observed a reduction of 14.30% in compressive strength when 2.0% PVA fibre was added into the plain mixture with a w/b ratio of 0.2. Besides, Wang et al. [37] found that the compressive strength of SHGC with 2.0% PVA fibre was about 9.70% and 7.30% lower than that containing 1.5% PVA fibre at 7 d and 28 d, respectively.

Similarly, as shown in Fig. 11a, the addition of RTP fibres also had a negative impact on compressive strength of SHGC. For instance, the 28-d compressive strength of P1.5R0.5 was around 45.7 MPa which was 10.43% lower than that of P1.5R0. Such weakening effect in compressive strength caused by RTP fibres was also found for cementitious composites [44, 47], which can be attributed to the weaker fibre-matrix interaction and lower stiffness of RTP fibres. In addition, the

rubber granules attaching the RTP fibres may also contribute to the reduction in compressive strength. Nevertheless, in this study, the RTP fibres were pre-treated to remove most of the attached rubber granules, which would effectively minimise the negative effect due to the rubber granules. Therefore, SHGC containing hybrid PVA and RTP fibres (except P1.25R0.75) exhibited even higher compressive strength (3.96-9.21% higher) than SHGC with 2.0% PVA fibre, indicating that replacing a certain content of PVA fibres by RTP fibres can help mitigate the loss of compressive strength in SHGC due to the addition of PVA fibres. Regardless of incorporating mono PVA or hybrid fibres, the compressive failure of SHGC is not sudden as compared with the brittle failure of plain matrix mixture. As displayed in Fig. 11b, P0R0 exhibited a significant damage after being subjected to a compressive load, leading to a triangular failure pattern with oblique cracks. By contrast, only some vertical cracks can be observed on the failure surface of SHGC, remaining its original shape (Fig. 11c). A similar phenomenon was reported in [37, 80] that the original cubic shape of SHGC was maintained after the compressive failure owing to the bridging capacity of the fibres. Compared to the plain matrix mixture, the compressive strength of SHGC is lower while its ultimate compressive strain may be higher [79] that needs to be confirmed by measuring the longitudinal strain of the specimen during the compressive loading. In summary, the compressive strength of SHGC containing both PVA and RTP fibres is acceptable for general construction purposes.

3.4. Uniaxial tensile behaviour

3.4.1. Stress-strain response

Fig. 12 depicts the tensile stress-strain curves of all mixtures. Typically, the tensile stress-strain curve consists of two distinct regions, an elastic region and a strain hardening or softening region. During the elastic region, the tensile stress of the tested sample increases rapidly and linearly with a small change of strain before reaching the elastic limit that is regarded as the transition point between the linearity region and non-linearity region, also known as first cracking strength (f_{fc}) [81]. After that, the tested sample either experiences steady rising stress (strain hardening) or gradual decreasing stress (strain softening) with the increase of strain. The highest point of stress is tensile strength (f_t) and the corresponding strain is tensile strain capacity (ε_t). As seen in Fig. 12, P0R0 had a very brittle tensile behaviour and failed immediately after reaching its tensile limit. Remarkably, P1.5R0, P2.0R0, P1.75R0.25 and P1.5R0.5 displayed an apparent strain hardening phenomenon while the strain hardening behaviour of P1.0R0 and P1.25R0.75 was not pronounced. P1.0R1.0 even lost the strain hardening feature but exhibited strain softening behaviour after reaching f_{fc}. Regarding the effects of PVA (Fig. 12a) and RTP fibres (Fig. 12b), it can be found that with the increase of PVA fibre dosage, the strain hardening region was consistently prolonged whereas the strain hardening behaviour was weakened when more RTP fibres replaced PVA fibres. The tensile properties

including f_{fc}, f_t, ε_t and strain energy derived from the stress-strain curves are discussed below to further estimate the effect of fibres on the tensile behaviour of SHGC.

3.4.2. Tensile properties

Fig. 13 shows f_{fc} and f_t of all mixtures. f_{fc} of the composite is mainly dependent on its matrix and no clear trend of change in f_{fc} of SHGC can be found when the fibre dosage altered. All SHGC mixtures had f_{fc} ranging from 1.28 MPa to 2.42 MPa, which mostly was higher than f_{fc} of P0R0 because of the fibre bridging effect inside the composite [82]. P2.0R0 had the highest f_{fc} of 2.42 MPa, which is consistent with the finding by Ohno and Li [11] that f_{fc} of SHGC was increased by 1.0 MPa when the PVA fibre dosage changed from 1.0% to 2.0%. In comparison with P2.0R0, f_{fc} of SHGC containing RTP fibres was lower, which can be assigned to the increase of pre-existing flaws when more RTP fibres were incorporated. This can be evidenced that f_{fc} of P1.0R1.0 was 23.80% lower than that of P1.0R0 (Fig. 13a). Converse to compressive strength, the increase of PVA fibre dosage led to an increase in f_t of SHGC by about 57.18-123.87% as compared with P0R0 (Fig. 13b). It is worth noting that f_t of P2.0R0 (3.4 MPa) in this study was comparable to that of FA-GGBS based SHGC with a modulus of AL of 1.5 [26]. The significant enhancement in f_t due to the increase of PVA fibre dosage can be associated with the fibre distribution and fibre bridging action. The fibres inside the dog-bone shaped specimen can be regarded as two-dimensional randomly distributed [34], suggesting that when more PVA fibres are present, the number of efficient bridging fibres tends to increase, in turn, significantly improving f_t of SHGC. By contrast, adding RTP fibres into SHGC decreased f_t of the whole composites. More specifically, f_t of P1.0R1.0 was only 1.68 MPa which was 29.58% lower than that of P1.0R0. However, the negative influence of 0.5% RTP fibre on f_t of SHGC was limited, only 3.81% lower as compared with P1.5R0. The loss in f_t due to the addition of recycled fibres is in consistence with previous studies about SHCC [33, 34]. Following the same trend of f_{fc}, a lower f_t of SHGC can be found when SHGC contained more RTP fibres, which can be mainly ascribed to the lower bridging stress of RTP fibres in comparison with PVA fibres. Nevertheless, all SHGC specimens containing hybrid PVA and RTP fibres showed higher f_t than P0R0.

Fig. 14 shows ε_t of all mixtures. It can be observed that the influence of fibres on ε_t is similar to that on f_t. For instance, ε_t of SHGC was increased with the increasing PVA fibre dosage, where the values of P1.0R0, P1.5R0 and P2.0R0 were about 16-255 times larger than that of P0R0 (only 0.01%). P2.0R0 had ε_t of around 3.04% which is slightly higher than that of SHCC M45 (2.49%), reported by Wang and Li [83]. Although SHGC containing RTP fibres showed a lower ε_t than P2.0R0, they still outperformed P0R0 by 2-188 times. On the other hand, the strain energy can be also used to reflect the strain hardening degree of SHGC, which is defined as the energy dissipation capacity per

unit volume during the strain hardening region and can be calculated by integrating the ascending branch of the tensile stress-strain curve, as illustrated in Fig. 15a. The calculated strain energy of all mixtures is shown in Fig. 15b, which agrees well with the results of f_t and ε_t, as discussed above. P2.0R0 had the highest strain energy of about 89.94 kJ/m^3, representing the best strain hardening performance.

In summary, it can be suggested that replacing a certain content of PVA fibres in SHGC with RTP fibres can ensure adequate tensile performance for certain applications. For instance, P1.75R0.25 outperformed P1.5R0 and P1.0R0 in terms of all relevant tensile properties.

3.4.3. Cracking analysis

The typical tensile fracture patterns of all mixtures are illustrated in Fig. 16. It should be noted that the image of P0R0 was taken after tensile failure while the images of SHGC specimens were captured before unloading. As mentioned in Section 2.4.4, only the cracks that appeared inside the gauge length were considered in this study and the dimension of the region for analysing the cracks was 30 mm × 80 mm (Fig. 16b-h). The cracking patterns here are consistent with the stress-strain curves shown in Fig. 12 that obvious multiple cracking features can be observed for P1.5R0, P2.0R0, P1.75R0.25 and P1.5R0.5 (Fig. 16c-f) along with clear strain hardening features. Only several cracks can be observed for P1.0R0, P1.25R0.75 and P1.0R1.0. Independent of fibre type and fibre dosage, the presence of fibres improved the post-cracking behaviour of SHGC compared to the brittle failure of P0R0 (Fig. 16a). Besides, more uniformly distributed cracks can be found in P2.0R0, which are consistent with its best tensile properties, as discussed previously.

Table 6 lists the residual crack number and crack width of SHGC after the removal of tensile load. The actual crack widths should be smaller than the residual crack widths as many micro-cracks are closed upon the removal of tensile load [84]. There exists a similar trend of residual crack number with that of ε_t. A large standard deviation can be noticed for P1.5R0, mainly due to the random fibre distribution between each sample even from the same batch of mixing [26]. The performance of P2.0R0 was more stable as the coefficient of variation (COV) of the residual crack number is only 3.57%. On the other hand, the residual crack width of SHGC was smaller when more PVA fibres were present, where the crack-controlling behaviour was affected by the fibre-matrix interface. As seen in Fig. 17a, at the fracture surface of SHGC, most of PVA fibres were pulled out, implying that the bond strength between fibres and matrix is adequate to avoid fibre rupture. Such fibre-matrix interface behaviour is favourable for improving the tensile behaviour and restraining the crack width, given that the bridging fibre has high enough tensile strength [85]. However, some PVA fibres were ruptured due to their inherent large chemical bond. Although RTP fibres also experienced pull-out behaviour during the tensile loading (Fig. 17b), the short length and low tensile strength (see Table 3) limit the crack-controlling behaviour of the whole composite. Thus, a larger crack width was found

in SHGC when more RTP fibres were added. This regard will be further discussed in Section 3.5 through the analysis of micromechanical and microstructural investigation.

In summary, the average residual crack widths of P1.5R0, P2.0R0, P1.75R0.25 and P1.5R0.5 were in the range of 29.8-39.2 μm, similar to those reported in a typical SHCC (60 μm) [84] and other SHGC (24.0-84.2 μm) [26, 85]. These tight crack widths indicate a strong crack-controlling ability of SHGC and are beneficial for many engineering properties, e.g., durability and self-healing performance [86]. However, further studies need to be conducted to confirm these benefits.

3.5. Micromechanical and microstructural investigation

Fig. 18 illustrates the representative tensile stress-crack opening curves of SHGC from the single crack direct tension tests. The experimental results of σ_0 and δ_0 are summarised in Table 7. The shape of the curves shown in Fig. 18 is affected by the dosage and properties of fibre and more importantly, the interface properties between fibre and matrix [1]. σ_0 is largely affected by the chemical bond and frictional bond between fibres and matrix [1, 26]. Thus, the increasing branch of the curve shown in Fig. 18 represents the required stress to overcome the chemical bond and pull out or rupture the fibres. With the increase of PVA fibre dosage, σ_0 of SHGC was consistently increased, which explains why P2.0R0 presented the best tensile performance as shown in Section 3.4. By contrast, increasing the RTP fibre replacement dosage led to a lower σ_0 in SHGC ranging from 1.08-2.02 MPa, which indicates that the tensile behaviour was diminished. Regarding δ_0, similar to σ_0, P2.0R0 had the highest value of 0.308 mm while there exhibited a general decreasing trend in δ_0 as the PVA fibre dosage in SHGC reduced. It was found that a higher δ_0 would benefit ε_t as higher stress is required to pull the fibres out [87].

To further interpret the results shown in Section 3.4 and verify whether the proposed mixtures here achieve a saturated strain hardening phenomenon, two strain hardening indices related to strength-based and energy-based criteria were determined (see Section 2.4.5). According to [88, 89], two following conditions need to be satisfied to achieve a saturated strain hardening behaviour: (1) $\sigma_0/\sigma_{fc} \geq 1.2$; (2) $J'_b/J_{tip} \geq 2.7$. The results of fracture toughness for P0R0 are shown in Table 8, which were used to determine J_{tip}. Table 9 lists the strain hardening indices of all SHGC mixtures. It can be found that P1.5R0, P2.0R0 and P1.75R0.25 satisfied the above two conditions, which are consistent with the stress-strain curves and cracking patterns shown in Fig. 12 and Fig. 16, respectively. P2.0R0 achieved the highest values in both indices, implying that it had a higher tendency to achieve a robust strain hardening feature along with a stable multiple cracking behaviour [88]. However, as observed from Table 9, P1.5R0.5 did not satisfy the requirements for a saturated strain hardening although its stress-strain curve showed an obvious strain hardening region. This phenomenon was also reported by Nematollahi et al. [16] that pronounced strain hardening and

multiple cracking were observed but the energy-based indices were only around 2.0. It is interesting to note that the strength-based index here was positively correlated to ε_t shown in Fig. 14, where a higher strength-based index corresponded to a higher ε_t, while the energy-based index showed a slight inconsistency. For instance, ε_t of P1.5R0.5 was considerably larger than that of P1.0R0 (0.96% versus 0.01%) but P1.0R0 possessed a higher energy-based index than P1.5R0.5 (see Table 9). This can be attributed to the deviations of the results, which are also reported in a previous study [85]. It is worth noting that the deviations tended to be higher when more RTP fibres were incorporated into SHGC, implying the important role of PVA fibres in tensile performance. Besides, this suggests that the tensile behaviour of SHGC containing hybrid fibre reinforcement may be less sensitive to the energy-based index.

Fig. 19 shows the SEM images of fibre morphology in mono-PVA fibre reinforced SHGC at the tensile fracture surfaces. Most of the PVA fibres experienced pull-out behaviour (Fig. 19a) which is in consistence with Fig. 17a. However, the ruptured PVA fibre with a necking end and several scratches can also be observed in Fig. 19b. Under adequate frictional stress, PVA fibres tended to be pulled out, where typically matrix fragments were attached with the fibre (Fig. 19c). The sufficient frictional stress can be also seen in Fig. 19d that no obvious gap was found between the fibre and matrix (red dash circles). Overall, not only the number of effective bridging fibres increases when the PVA fibre dosage increases but also the number of pull-out fibres increases. These ultimately result in a higher f_t and a larger ε_t in SHGC. On the other hand, Fig. 20 displays the SEM images of fibre morphology in hybrid PVA-RTP fibre reinforced SHGC. The pull-out RTP fibre can be identified which coincides with that shown in Fig. 17b. As explained previously, RTP fibres have a weaker bond with the matrix because of the hydrophobic feature, which can be supported by Fig. 20b that a clear void space was observed between the RTP fibre and the matrix. Besides, no pronounced matrix fragments attached to the RTP fibre. Therefore, the pull-out process can be easily facilitated and terminated quickly. This explains why more RTP fibres in SHGC would result in lower tensile properties and larger crack widths. However, when the incorporated RTP fibre content is appropriate, PVA and RTP fibres can form a synergistic effect to improve the crack-controlling behaviour of the whole composite.

4. Cost and environmental impact

As stated previously, the main objective of this work is to reduce the cost and improve the sustainability of SHGC through the partial replacement of PVA fibres. Thus, the effects of fibres on the total material cost, embodied carbon and embodied energy were analysed. Table 10 lists the market price, embodied carbon and embodied energy of all ingredients needed for producing SHGC [11, 90-97]. The estimated total material cost of all mixtures in USD/m^3 is presented in Fig. 21. It can be found that the cost of PVA fibres constituted a considerably big part of the total material cost of

mono-PVA fibre reinforced SHGC and it was about 70.30% of the total cost. Replacing a certain content of PVA fibres (0.25-1.0%) with RTP fibres in SHGC significantly reduced the total cost by 8.63-34.52%. This large reduction can be attributed to the extremely lower cost of RTP fibres, which is only 1.62% that of PVA fibres. Although some other costs may be required for processing RTP fibres [98], the huge difference in material cost between RTP fibres and PVA fibres makes the SHGC containing RTP fibres promising and attractive for certain large-scale applications given the presence of adequate engineering properties.

Embodied carbon and embodied energy are considered as the major material sustainability indicators [34], which were considered to reflect the environmental impact of SHGC. Fig. 22 illustrates the embodied carbon and embodied energy of all mixtures. The corresponding results obtained from a typical M45 SHCC were also included in the figure for comparisons [99]. As seen in Fig. 22a, all mixtures presented a dramatically lower embodied carbon than a typical M45 SHCC as the matrix of SHCC containing a very high dosage of cement contributed significantly to the increase in embodied carbon. The embodied carbon of P2.0R0 was around 329 kg CO_2.eq/m^3, approximately 48.83% lower than that of a typical M45 SHCC. The embodied carbon gradually increased with the increase of PVA fibre dosage while no significant effect can be observed when PVA fibres were replaced with RTP fibres (purple trend line). On the other hand, as shown in Fig. 22b, the embodied energy of SHGC was comparable with that of SHCC. The embodied energy of SHGC presented a similar increasing trend as the PVA fibre dosage increased. By contrast, the embodied energy of SHGC reduced gradually with the rising RTP fibre replacement and the reduction was in the range of 4.06-16.23% compared to P2.0R0, which can be mainly ascribed to the lower embodied energy of recycled fibres, as given in Table 10. In addition, more solid wastes can be reduced when RTP fibres are incorporated. Overall, replacing PVA fibres with RTP fibres in SHGC can lead to an enhancement in the sustainability of construction materials considering the above results.

To comprehensively evaluate the feasibility of RTP fibres in SHGC, the overall performance between mono-fibre reinforced SHGC (P2.0R0) and hybrid fibre reinforced SHGC was compared. A comparison in terms of key engineering properties, total material cost and environmental impact is presented in Fig. 23, where all values of P2.0R0 were set as 1.0 while the results of hybrid PVA-RTP fibre reinforced SHGC were regulated based on those of P2.0R0. It can be found that apart from the improved sustainability and the reduced material cost, the dosage of RTP fibres in SHGC should be limited to ensure its applicability, resilience, and long-term durability. Overall, the addition of RTP fibres in SHGC is beneficial for compressive strength and especially drying shrinkage whereas the tensile behaviour is significantly diminished. P1.75R0.25 can be regarded as the most cost-effective mixture as it processed adequate engineering properties, lower cost and better sustainability as compared with P2.0R0. In addition, P1.5R0.5 with a ε_t of around 1.0% and the improved shrinkage-

resistance is also promising for certain applications, where better controlling of early-age cracking is required, e.g., repairing of existing structures.

5. Conclusions

To improve the cost-effectiveness and sustainability of fly ash-slag based SHGC with PVA fibres, this paper presents an experimental study on the feasibility of partially replacing PVA fibres with RTP fibres, considering the effects of PVA fibre dosage (1.0-2.0%) and RTP fibre replacement dosage (0.25-1.0%) on the engineering properties, material cost and environmental impact of SHGC. Based on the results of this study, the main conclusions can be drawn as follows:

- The presence of RTP fibres in SHGC can effectively reduce the drying shrinkage by 17.33% compared to that of SHGC with 2.0% PVA fibre, although lower flowability is observed in SHGC when more than 0.25% PVA fibre is replaced with RTP fibres. The reduced compressive strength in SHGC due to the presence of PVA fibres can be mitigated by the incorporation of RTP fibres.
- The tensile properties of SHGC including f_t, $\varepsilon_t$and strain energy are considerably improved with the increase of PVA fibre dosage while these properties are reduced when more PVA fibres are replaced with RTP fibres. SHGC mixtures with mono PVA fibre (1.5% and 2.0%) and hybrid fibres (1.75% PVA and 0.25% RTP) present robust tensile strain hardening and saturated multiple cracking features according to the results of stress-strain response, fracture pattern and strain hardening indices.
- SEM micrographs indicate more pull-out PVA fibres appear at the tensile fracture surface of SHGC, which is favourable for the improvement of tensile properties, while a weaker bond is observed at the interface between RTP fibre and matrix, resulting in poor tensile behaviour of SHGC.
- The presence of RTP fibres decreases the material cost and embodied energy of SHGC by 8.63-34.52% and 4.06-16.23%, respectively. A comparison of the overall composite performance between mono-PVA fibre reinforced SHGC and hybrid PVA-RTP fibre reinforced SHGC, the most cost-effective combination for SHGC is 1.75% PVA fibre and 0.25% RTP fibre, as it exhibits adequate engineering properties, lower material cost and better sustainability in comparison with SHGC with 2.0% PVA fibre.

This paper reveals a large potential of producing a cost-effective and sustainable fly ash-slag based SHGC via the replacement of PVA fibres with RTP fibres. Although the use of RTP fibres is not effective in improving the static mechanical properties of SHGC, it can greatly restrain the drying shrinkage. Satisfactory engineering properties (e.g. ε_t of 1.0% or above) are still achievable when 0.5% PVA fibre is replaced by RTP fibres in SHGC, which can be useful for certain practical applications. Besides, it is expected that the addition of RTP fibres can enhance the dynamic mechanical properties of SHGC [46, 48]. Therefore, it is vital to investigate the effect of RTP fibre

on the dynamic behaviour of SHGC with a wide range of strain rates. Moreover, the drying shrinkage of hybrid fibre reinforced SHGC is still a concern as compared with traditional SHCC and thus it is important to find an effective strategy to further reduce the drying shrinkage of SHGC. These are subjects of ongoing works and will be presented in future publications.

Acknowledgements

The authors gratefully acknowledge the financial support from the Engineering and Physical Sciences Research Council (EPSRC), UK under Grant No. EP/R041504/1 and the Royal Society, UK under Award No. IEC\NSFC\191417 as well as the Visiting Researcher Fund Program of State Key Laboratory of Water Resources and Hydropower Engineering Science, China under Award No. 2019SGG01. The financial support provided by University College London (UCL) and China Scholarship Council (CSC) to the first author is gratefully acknowledged.

References

[1] V.C. Li, Engineered Cementitious Composites (ECC): Bendable Concrete for Sustainable and Resilient Infrastructure, Springer2019.

[2] V.C. Li, F.P. Bos, K. Yu, W. McGee, T.Y. Ng, S.C. Figueiredo, K. Nefs, V. Mechtcherine, V.N. Nerella, J. Pan, G.P.A.G. van Zijl, P.J. Kruger, On the emergence of 3D printable Engineered, Strain Hardening Cementitious Composites (ECC/SHCC), Cement and Concrete Research 132 (2020) 106038.

[3] A. Bentur, S. Mindess, Fibre reinforced cementitious composites, Crc Press2006.

[4] V.C. Li, C.K. Leung, Steady-state and multiple cracking of short random fiber composites, J. Eng. Mech. 118(11) (1992) 2246-2264.

[5] V.C. Li, From micromechanics to structural engineering-the design of cementitous composites for civil engineering applications, Journal of Structural Mechanics and Earthquake Engineering 10 (1993) 37-48.

[6] K.-Q. Yu, J.-T. Yu, J.-G. Dai, Z.-D. Lu, S.P. Shah, Development of ultra-high performance engineered cementitious composites using polyethylene (PE) fibers, Construction and Building Materials 158 (2018) 217-227.

[7] Z. Zhang, F. Yang, J.-C. Liu, S. Wang, Eco-friendly high strength, high ductility engineered cementitious composites (ECC) with substitution of fly ash by rice husk ash, Cement and Concrete Research 137 (2020) 106200.

[8] T. Luukkonen, Z. Abdollahnejad, J. Yliniemi, P. Kinnunen, M. Illikainen, One-part alkali-activated materials: A review, Cement and Concrete Research 103 (2018) 21-34.

[9] P.J.M. Monteiro, S.A. Miller, A. Horvath, Towards sustainable concrete, Nature Materials 16(7) (2017) 698-699.

[10] M. Ohno, V.C. Li, A feasibility study of strain hardening fiber reinforced fly ash-based geopolymer composites, Construction and Building Materials 57 (2014) 163-168.
[11] M. Ohno, V.C. Li, An integrated design method of Engineered Geopolymer Composite, Cement and Concrete Composites 88 (2018) 73-85.
[12] B. Nematollahi, J. Sanjayan, F.U.A. Shaikh, Comparative deflection hardening behavior of short fiber reinforced geopolymer composites, Construction and Building Materials 70 (2014) 54-64.
[13] B. Nematollahi, J. Sanjayan, F.U.A. Shaikh, Tensile Strain Hardening Behavior of PVA Fiber-Reinforced Engineered Geopolymer Composite, Journal of Materials in Civil Engineering 27(10) (2015) 1-12.
[14] B. Nematollahi, J. Sanjayan, F.U.A. Shaikh, Matrix design of strain hardening fiber reinforced engineered geopolymer composite, Composites Part B: Engineering 89 (2016) 253-265.
[15] M. Farooq, A. Bhutta, N. Banthia, Tensile performance of eco-friendly ductile geopolymer composites (EDGC) incorporating different micro-fibers, Cement and Concrete Composites 103 (2019) 183-192.
[16] B. Nematollahi, J. Sanjayan, J. Qiu, E.-H. Yang, Micromechanics-based investigation of a sustainable ambient temperature cured one-part strain hardening geopolymer composite, Construction and Building Materials 131 (2017) 552-563.
[17] B.Y. Lee, C.-G. Cho, H.-J. Lim, J.-K. Song, K.-H. Yang, V.C. Li, Strain hardening fiber reinforced alkali-activated mortar – A feasibility study, Construction and Building Materials 37 (2012) 15-20.
[18] S.-J. Choi, J.-I. Choi, J.-K. Song, B.Y. Lee, Rheological and mechanical properties of fiber-reinforced alkali-activated composite, Construction and Building Materials 96 (2015) 112-118.
[19] J.-I. Choi, H.H. Nguyễn, S.L. Cha, M. Li, B.Y. Lee, Composite properties of calcium-based alkali-activated slag composites reinforced by different types of polyethylene fibers and micromechanical analysis, Construction and Building Materials 273 (2021) 121760.
[20] J.-I. Choi, H.-K. Kim, B.Y. Lee, Mechanical and Fiber-Bridging Behavior of Slag-Based Composite with High Tensile Ductility, Applied Sciences 10(12) (2020).
[21] G. Fang, M. Zhang, Multiscale micromechanical analysis of alkali-activated fly ash-slag paste, Cement and Concrete Research 135 (2020) 106141.
[22] H. Ye, A. Radlińska, Shrinkage mechanisms of alkali-activated slag, Cement and Concrete Research 88 (2016) 126-135.
[23] S.-D. Wang, X.-C. Pu, K.L. Scrivener, P.L. Pratt, Alkali-activated slag cement and concrete: a review of properties and problems, 7(27) (1995) 93-102.

[24] B. Nematollahi, J. Sanjayan, J. Qiu, E.-H. Yang, High ductile behavior of a polyethylene fiber-reinforced one-part geopolymer composite: A micromechanics-based investigation, Archives of Civil and Mechanical Engineering 17(3) (2017) 555-563.
[25] Y. Ling, K. Wang, W. Li, G. Shi, P. Lu, Effect of slag on the mechanical properties and bond strength of fly ash-based engineered geopolymer composites, Composites Part B: Engineering 164 (2019) 747-757.
[26] S. Zhang, V.C. Li, G. Ye, Micromechanics-guided development of a slag/fly ash-based strain-hardening geopolymer composite, Cement and Concrete Composites 109 (2020) 103510.
[27] Y. Wang, Y. Wang, M. Zhang, Effect of sand content on engineering properties of fly ash-slag based strain hardening geopolymer composites, Journal of Building Engineering 34 (2021) 101951.
[28] J. Yu, C.K. Leung, Strength improvement of strain-hardening cementitious composites with ultrahigh-volume fly ash, Journal of Materials in Civil Engineering 29 (2017) 05017003.
[29] D. Zhang, J. Yu, H. Wu, B. Jaworska, B.R. Ellis, V.C. Li, Discontinuous micro-fibers as intrinsic reinforcement for ductile Engineered Cementitious Composites (ECC), Composites Part B: Engineering 184 (2020) 107741.
[30] V.C. Li, Engineered Cementitious Composites (ECC) - material, structural, and durability performance, in: E. Nawy (Ed.), Concrete Construction Engineering Handbook, CRC Press, Boca Raton, 2008.
[31] R. Merli, M. Preziosi, A. Acampora, M.C. Lucchetti, E. Petrucci, Recycled fibers in reinforced concrete: A systematic literature review, Journal of Cleaner Production 248 (2019) 119207.
[32] K.M. Liew, A. Akbar, The recent progress of recycled steel fiber reinforced concrete, Construction and Building Materials 232 (2020) 117232.
[33] W.-C. Choi, H.-D. Yun, J.-W. Kang, S.-W. Kim, Development of recycled strain-hardening cement-based composite (SHCC) for sustainable infrastructures, Composites Part B: Engineering 43(2) (2012) 627-635.
[34] J. Yu, J. Yao, X. Lin, H. Li, J.Y.K. Lam, C.K.Y. Leung, I.M.L. Sham, K. Shih, Tensile performance of sustainable Strain-Hardening Cementitious Composites with hybrid PVA and recycled PET fibers, Cement and Concrete Research 107 (2018) 110-123.
[35] C. Lu, J. Yu, C.K.Y. Leung, Tensile performance and impact resistance of Strain Hardening Cementitious Composites (SHCC) with recycled fibers, Construction and Building Materials 171 (2018) 566-576.
[36] B.S. Mohammed, V.C. Khed, M.S. Liew, Optimization of hybrid fibres in engineered cementitious composites, Construction and Building Materials 190 (2018) 24-37.

[37] Y. Wang, C.L. Chan, S.H. Leong, M. Zhang, Engineering properties of strain hardening geopolymer composites with hybrid polyvinyl alcohol and recycled steel fibres, Construction and Building Materials 261 (2020) 120585.
[38] G. Malarvizhi, N. Senthul, C. Kamaraj, A study on Recycling of crumb rubber and low density polyethylene blend on stone matrix asphalt, International Journal of Science and Research 2(10) (2012).
[39] B.S. Thomas, R.C. Gupta, A comprehensive review on the applications of waste tire rubber in cement concrete, Renewable and Sustainable Energy Reviews 54 (2016) 1323-1333.
[40] A. Baričević, M. Jelčić Rukavina, M. Pezer, N. Štirmer, Influence of recycled tire polymer fibers on concrete properties, Cement and Concrete Composites 91 (2018) 29-41.
[41] S.-S. Huang, H. Angelakopoulos, K. Pilakoutas, I. Burgess, Reused tyre polymer fibre for fire-spalling mitigation, Applications of Structural Fire Engineering, 2015.
[42] M. Serdar, A. Baričević, M. Jelčić Rukavina, M. Pezer, D. Bjegović, N. Štirmer, Shrinkage Behaviour of Fibre Reinforced Concrete with Recycled Tyre Polymer Fibres, International Journal of Polymer Science 2015 (2015) 1-9.
[43] O. Onuaguluchi, N. Banthia, Durability performance of polymeric scrap tire fibers and its reinforced cement mortar, Materials and Structures 50(2) (2017).
[44] M. Chen, H. Zhong, L. Chen, Y. Zhang, M. Zhang, Engineering properties and sustainability assessment of recycled fibre reinforced rubberised cementitious composite, Journal of Cleaner Production 278 (2021) 123996.
[45] A. Baricevic, M. Pezer, M. Jelcic Rukavina, M. Serdar, N. Stirmer, Effect of polymer fibers recycled from waste tires on properties of wet-sprayed concrete, Construction and Building Materials 176 (2018) 135-144.
[46] M. Chen, W. Chen, H. Zhong, D. Chi, Y. Wang, M. Zhang, Experimental study on dynamic compressive behaviour of recycled tyre polymer fibre reinforced concrete, Cement and Concrete Composites 98 (2019) 95-112.
[47] M. Chen, H. Zhong, M. Zhang, Flexural fatigue behaviour of recycled tyre polymer fibre reinforced concrete, Cement and Concrete Composites 105 (2020) 103441.
[48] M. Chen, H. Zhong, H. Wang, M. Zhang, Behaviour of recycled tyre polymer fibre reinforced concrete under dynamic splitting tension, Cement and Concrete Composites 114 (2020) 103764.
[49] ASTM C618-17a, Standard Specification for Coal Fly Ash and Raw or Calcined Natural Pozzolan for Use in Concrete, ASTM International, West Conshohocken, PA, 2017.
[50] J.J. Chang, A study on the setting characteristics of sodium silicate-activated slag pastes, Cement and Concrete Research 33(7) (2003) 1005-1011.

[51] M.I. Khan, G. Fares, S. Mourad, W.J.J.o.M.i.C.E. Abbass, Optimized Fresh and Hardened Properties of Strain-Hardening Cementitious Composites: Effect of Sand Size and Workability, Journal of Materials in Civil Engineering 28(12) (2016).
[52] S. Vahur, U. Knuutinen, I. Leito, ATR-FT-IR spectroscopy in the region of 500–230cm−1 for identification of inorganic red pigments, Spectrochimica Acta Part A: Molecular and Biomolecular Spectroscopy 73(4) (2009) 764-771.
[53] ASTM E1252-98, Standard Practice for General Techniques for Obtaining Infrared Spectra for Qualitative Analysis, ASTM International, West Conshohocken, PA, 2013.
[54] K.C. Cole, A. Ajji, É. Pellerin, New insights into the development of ordered structure in poly(ethylene terephthalate), II Results from transmission infrared spectroscopy of thin films, 184(1) (2002) 1-18.
[55] L. Meng, X. Xu, B. Bai, M. Ma, S. Li, N. Hu, H. Wang, Y. Suo, Surface carboxyl-activated polyester (PET) fibers decorated with glucose carbon microspheres and their enhanced selective adsorption for dyes, J. Phys. Chem. Solids 123 (2018) 378-388.
[56] M.-X. Guo, S.-W. Bian, F. Shao, S. Liu, Y.-H. Peng, Hydrothermal synthesis and electrochemical performance of MnO2/graphene/polyester composite electrode materials for flexible supercapacitors, Electrochim. Acta 209 (2016) 486-497.
[57] M. Mecozzi, L. Nisini, The differentiation of biodegradable and non-biodegradable polyethylene terephthalate (PET) samples by FTIR spectroscopy: A potential support for the structural differentiation of PET in environmental analysis, Infrared Physics & Technology 101 (2019) 119-126.
[58] J.R. Atkinson, F. Biddlestone, J.N. Hay, An investigation of glass formation and physical ageing in poly(ethylene terephthalate) by FT-IR spectroscopy, Polymer 41(18) (2000) 6965-6968.
[59] G. Fang, W.K. Ho, W. Tu, M. Zhang, Workability and mechanical properties of alkali-activated fly ash-slag concrete cured at ambient temperature, Construction and Building Materials 172 (2018) 476-487.
[60] J.G. Jang, N.K. Lee, H.K. Lee, Fresh and hardened properties of alkali-activated fly ash/slag pastes with superplasticizers, Construction and Building Materials 50 (2014) 169-176.
[61] Y. Jing, Multi-scale study on strain-hardening cementitious composites with hybrid fibers, The Hong Kong University of Science and Technology, 2017.
[62] ASTM C1437-15, Standard Test Method for Flow of Hydraulic Cement Mortar, ASTM International, West Conshohocken, PA, United States, 2015.
[63] ASTM C490-17, Standard Practice for Use of Apparatus for the Determination of Length Change of Hardened Cement Paste, Mortar, and Concrete, ASTM International, West Conshohocken, PA, United States, 2017.

[64] ASTM C109/C109M-20b, Standard Test Method for Compressive Strength of Hydraulic Cement Mortars (Using 2-in . or [50-mm] Cube Specimens), ASTM International, West Conshohocken, PA, 2020.
[65] Japan Society of Civil Engineers, Recommendations for design and construction of high performance fiber reinforced cement composites with multiple fine cracks (HPFRCC), Concrete Engineering Series No. 82 (2008).
[66] T. Kanda, V.C. Li, New micromechanics design theory for pseudostrain hardening cementitious composite, J. Eng. Mech. 125(4) (1999) 373-381.
[67] D.B. Marshall, B.N. Cox, A J-integral method for calculating steady-state matrix cracking stresses in composites, Mech. Mater. 7(2) (1988) 127-133.
[68] RILEM FMC-50, Determination of the fracture energy of mortar and concrete by means of three-point bend tests on notched beams, 18(4) (1985) 287-290.
[69] S. Xu, H.W. Reinhardt, Determination of double-K criterion for crack propagation in quasi-brittle fracture, Part II: Analytical evaluating and practical measuring methods for three-point bending notched beams, International Journal of Fracture 98(2) (1999) 151-177.
[70] N. Ranjbar, M. Zhang, Fiber-reinforced geopolymer composites: A review, Cement and Concrete Composites 107 (2020) 103498.
[71] R. Swamy, P. Mangat, Influence of fibre-aggregate interaction on some properties of steel fibre reinforced concrete, Matériaux et Construction 7(5) (1974) 307-314.
[72] G. Masi, W.D.A. Rickard, M.C. Bignozzi, A. van Riessen, The effect of organic and inorganic fibres on the mechanical and thermal properties of aluminate activated geopolymers, Composites Part B: Engineering 76 (2015) 218-228.
[73] J. Zhang, C. Gong, Z. Guo, M. Zhang, Engineered cementitious composite with characteristic of low drying shrinkage, Cement and Concrete Research 39(4) (2009) 303-312.
[74] N.K. Lee, J.G. Jang, H.K. Lee, Shrinkage characteristics of alkali-activated fly ash/slag paste and mortar at early ages, Cement and Concrete Composites 53 (2014) 239-248.
[75] V. Afroughsabet, S. Teng, Experiments on drying shrinkage and creep of high performance hybrid-fiber-reinforced concrete, Cement and Concrete Composites 106 (2020) 103481.
[76] B.-C. Lyu, C. Ding, L.-P. Guo, B. Chen, A.-g. Wang, Basic performances and potential research problems of strain hardening geopolymer composites: A critical review, Construction and Building Materials 287 (2021) 123030.
[77] P.-m. Zhan, Z.-h. He, Application of shrinkage reducing admixture in concrete: A review, Construction and Building Materials 201 (2019) 676-690.
[78] Y. Ling, K. Wang, C. Fu, Shrinkage behavior of fly ash based geopolymer pastes with and without shrinkage reducing admixture, Cement and Concrete Composites 98 (2019) 74-82.

[79] K. Yu, Y. Ding, Y.X. Zhang, Size effects on tensile properties and compressive strength of engineered cementitious composites, Cement and Concrete Composites 113 (2020) 103691.
[80] L.-l. Kan, W.-s. Wang, W.-d. Liu, M. Wu, Development and characterization of fly ash based PVA fiber reinforced Engineered Geopolymer Composites incorporating metakaolin, Cement and Concrete Composites 108 (2020) 103521.
[81] Y. Alrefaei, J.-G. Dai, Tensile behavior and microstructure of hybrid fiber ambient cured one-part engineered geopolymer composites, Construction and Building Materials 184 (2018) 419-431.
[82] E. Yang, V.C. Li, Numerical study on steady-state cracking of composites, Composites Science and Technology 67(2) (2007) 151-156.
[83] S. Wang, V.C. Li, Engineered cementitious composites with high-volume fly ash, ACI Mater. J. 104(3) (2007) 233-241.
[84] V.C. Li, S. Wang, C. Wu, Tensile strain-hardening behavior of polyvinyl alcohol engineered cementitious composite (PVA-ECC), ACI Mater. J. 98(6) (2001) 483-492.
[85] Y. Zhao, T. Shi, L. Cao, L. Kan, M. Wu, Influence of steel slag on the properties of alkali-activated fly ash and blast-furnace slag based fiber reinforced composites, Cement and Concrete Composites 116 (2021) 103875.
[86] J. Qiu, H.S. Tan, E.-H. Yang, Coupled effects of crack width, slag content, and conditioning alkalinity on autogenous healing of engineered cementitious composites, Cement and Concrete Composites 73 (2016) 203-212.
[87] K.-Q. Yu, W.-J. Zhu, Y. Ding, Z.-D. Lu, J.-t. Yu, J.-Z. Xiao, Micro-structural and mechanical properties of ultra-high performance engineered cementitious composites (UHP-ECC) incorporation of recycled fine powder (RFP), Cement and Concrete Research 124 (2019) 105813.
[88] T. Kanda, V.C. Li, Practical design criteria for saturated pseudo strain hardening behavior in ECC, Journal of advanced concrete technology 4 (2006) 59-72.
[89] T. Kanda, V.C. Li, Multiple cracking sequence and saturation in fiber reinforced cementitious composites, Concrete Research and Technology 9 (1998) 19-33.
[90] Z. Abdollahnejad, F. Pacheco-Torgal, T. Félix, W. Tahri, J. Barroso Aguiar, Mix design, properties and cost analysis of fly ash-based geopolymer foam, Construction and Building Materials 80 (2015) 18-30.
[91] A. Rafeet, R. Vinai, M. Soutsos, W. Sha, Guidelines for mix proportioning of fly ash/GGBS based alkali activated concretes, Construction and Building Materials 147 (2017) 130-142.
[92] D. Zhang, B. Jaworska, H. Zhu, K. Dahlquist, V.C. Li, Engineered Cementitious Composites (ECC) with limestone calcined clay cement (LC3), Cement and Concrete Composites 114 (2020) 103766.

[93] G. Hammond, C. Jones, F. Lowrie, P. Tse, Inventory of carbon & energy: ICE, Sustainable Energy Research Team, Department of Mechanical Engineering 2008.
[94] R. Ranade, Advanced cementitious composite development for resilient and sustainable infrastructure, University of Michigan, 2014.
[95] M. Fawer, M. Concannon, W. Rieber, Life cycle inventories for the production of sodium silicates, The International Journal of Life Cycle Assessment 4(4) (1999) 207.
[96] R. Frazão, R. Fernandes, Comparative Analysis of the Life Cycle of AT Fibre-cement and NT Fibre-cement, International Chrysotile Association (2004).
[97] G.A. Keoleian, A. Kendall, J.E. Dettling, V.M. Smith, R.F. Chandler, M.D. Lepech, V.C. Li, Life cycle modeling of concrete bridge design: Comparison of engineered cementitious composite link slabs and conventional steel expansion joints, J. Infrastruct. Syst. 11 (2005) 51-60.
[98] S. Gigli, D. Landi, M. Germani, Cost-benefit analysis of a circular economy project: a study on a recycling system for end-of-life tyres, Journal of Cleaner Production 229 (2019) 680-694.
[99] J. Yu, H.-L. Wu, C.K.Y. Leung, Feasibility of using ultrahigh-volume limestone-calcined clay blend to develop sustainable medium-strength Engineered Cementitious Composites (ECC), Journal of Cleaner Production 262 (2020) 121343.

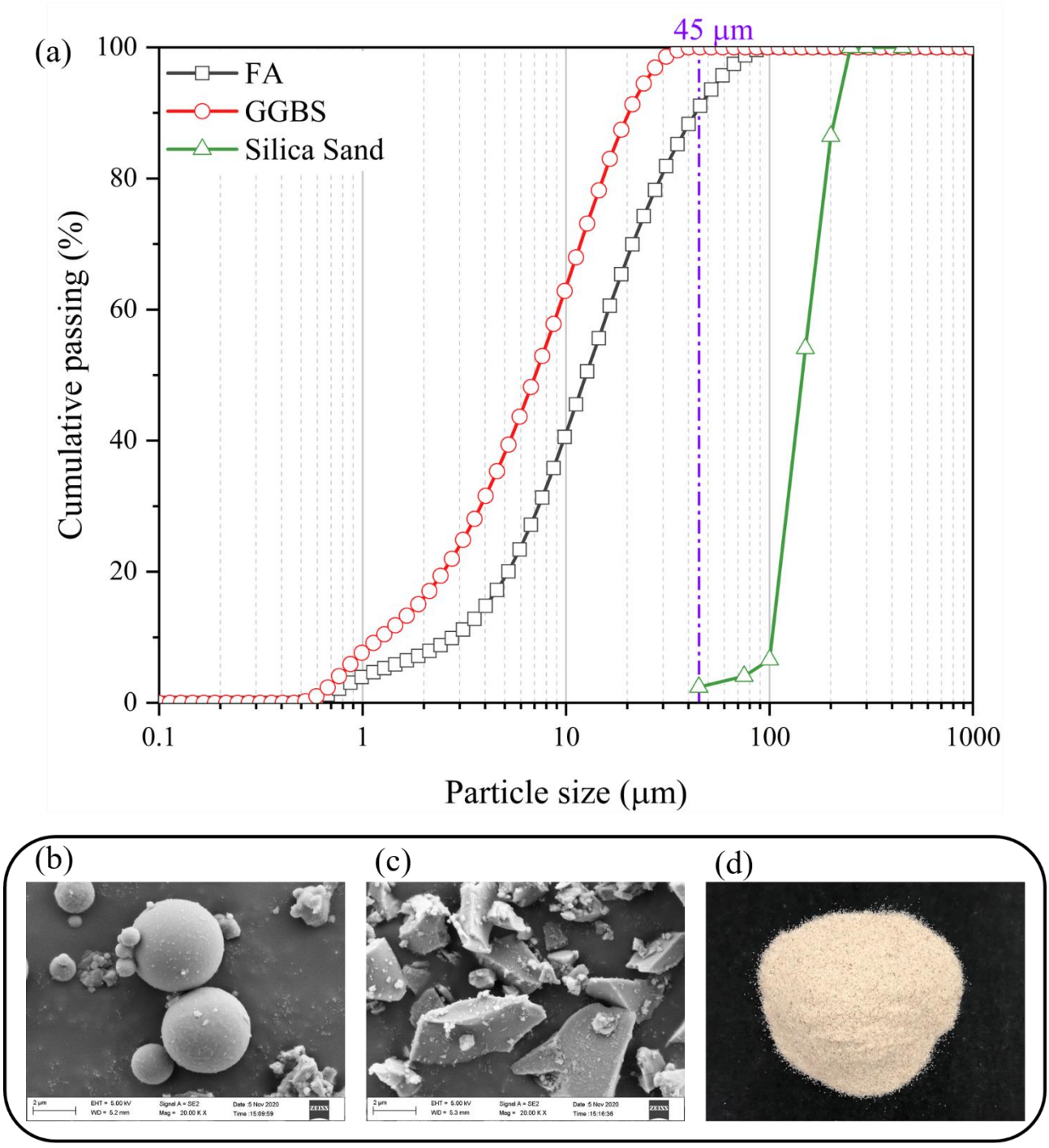

Fig. 1. Particle size distribution and morphology of matrix ingredients: (a) particle size distribution of fly ash (FA), ground granulated blast-furnace slag (GGBS) and silica sand; representative SEM images of (b) FA and (c) GGBS (magnification: 2000x); (d) digital camera image of silica sand.

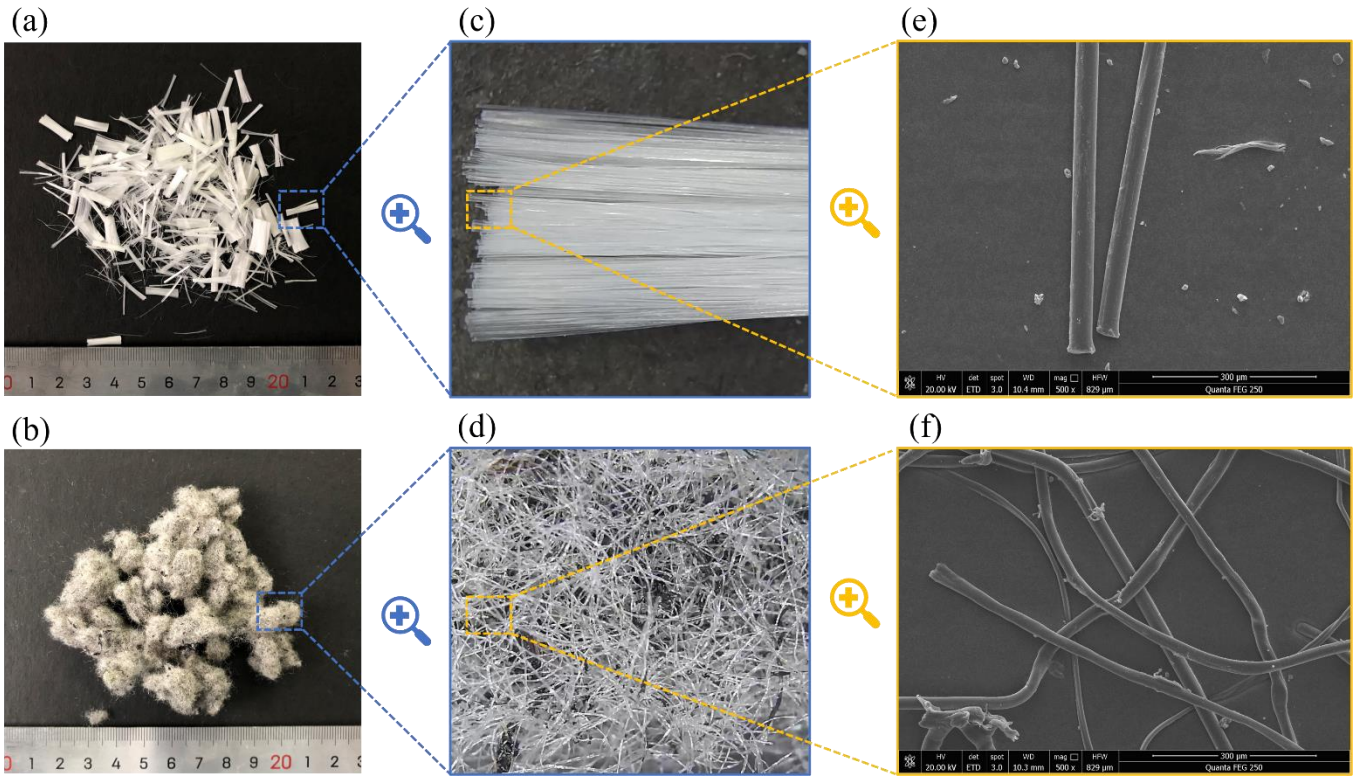

Fig. 2. Digital camera images of (a) PVA and (b) RTP fibres; Digital microscope images of (c) PVA and (d) RTP fibres; SEM images of (e) PVA and (f) RTP fibres (magnification: 500x).

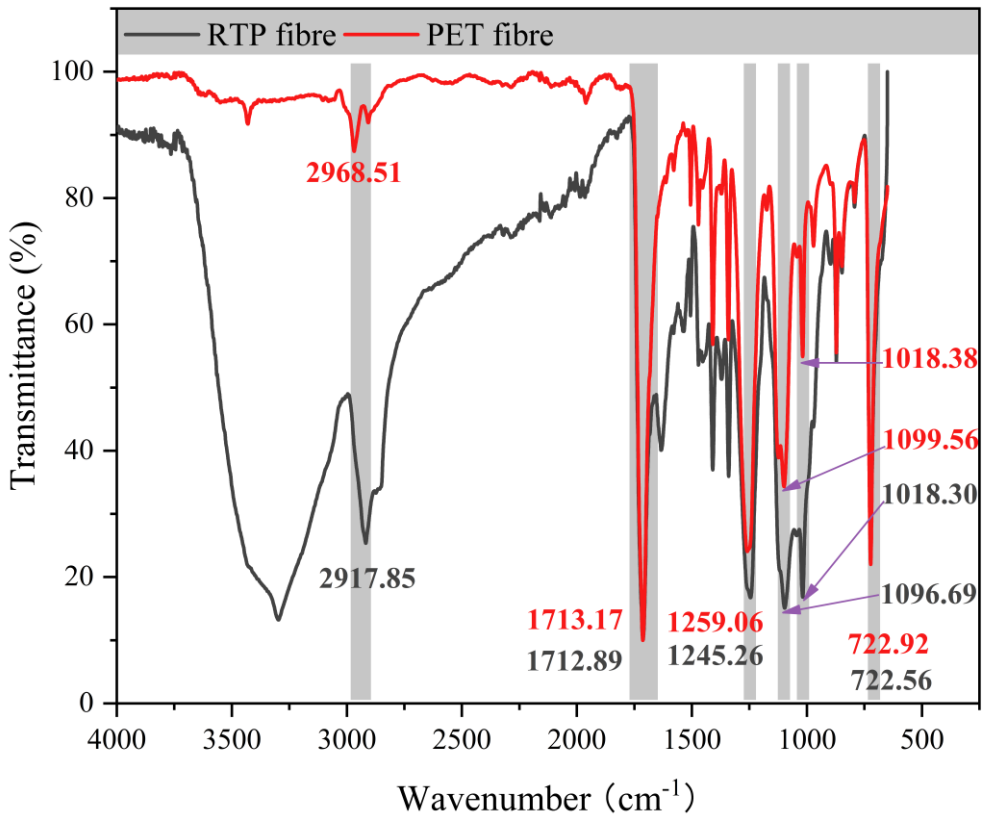

Fig. 3. Fourier transform infrared spectroscopy (FTIR) spectrum of RTP fibre and polyethylene terephthalate (PET) fibre.

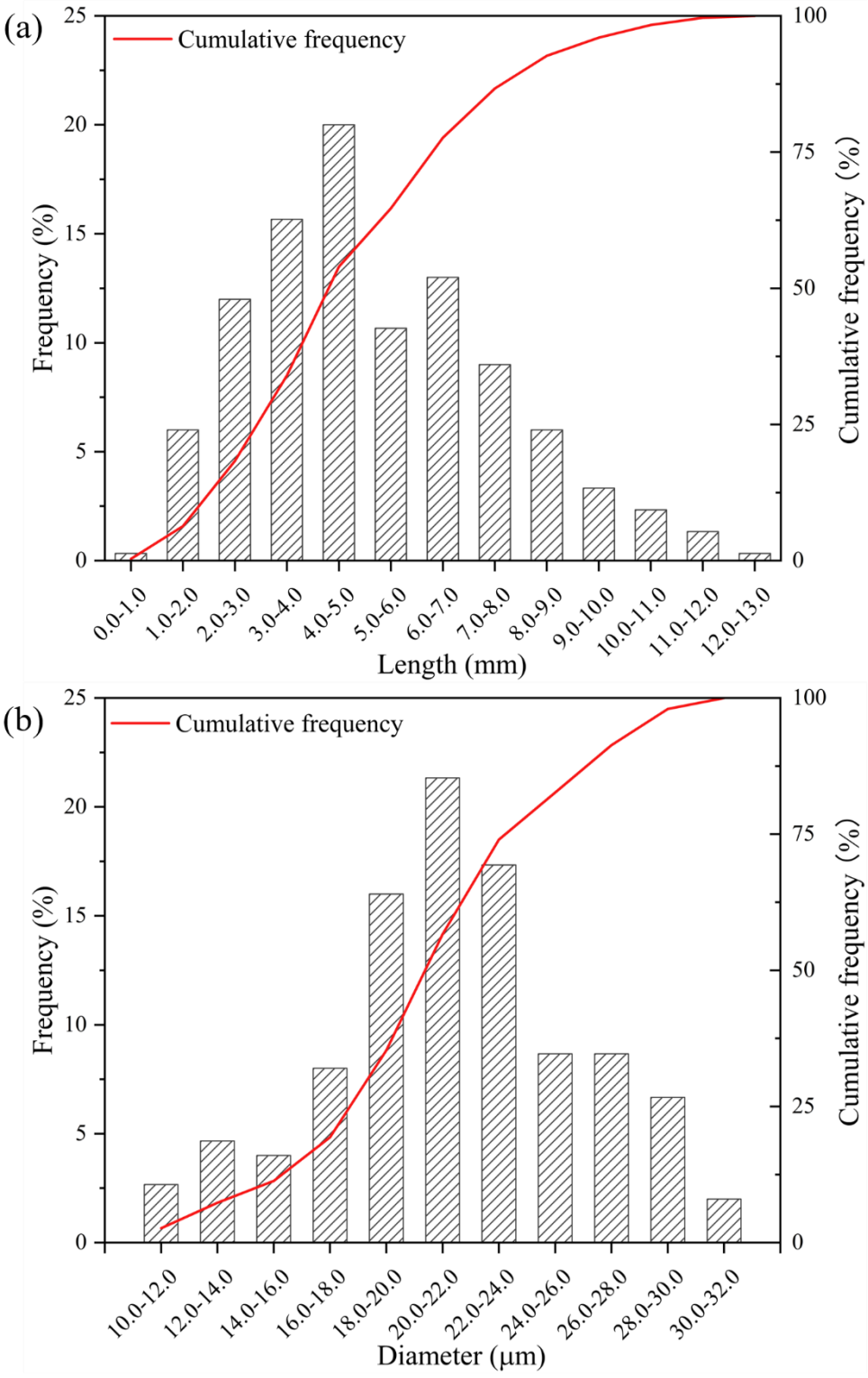

Fig. 4. Dimension of RTP fibres: (a) length distribution (in mm); (b) diameter distribution (in μm).

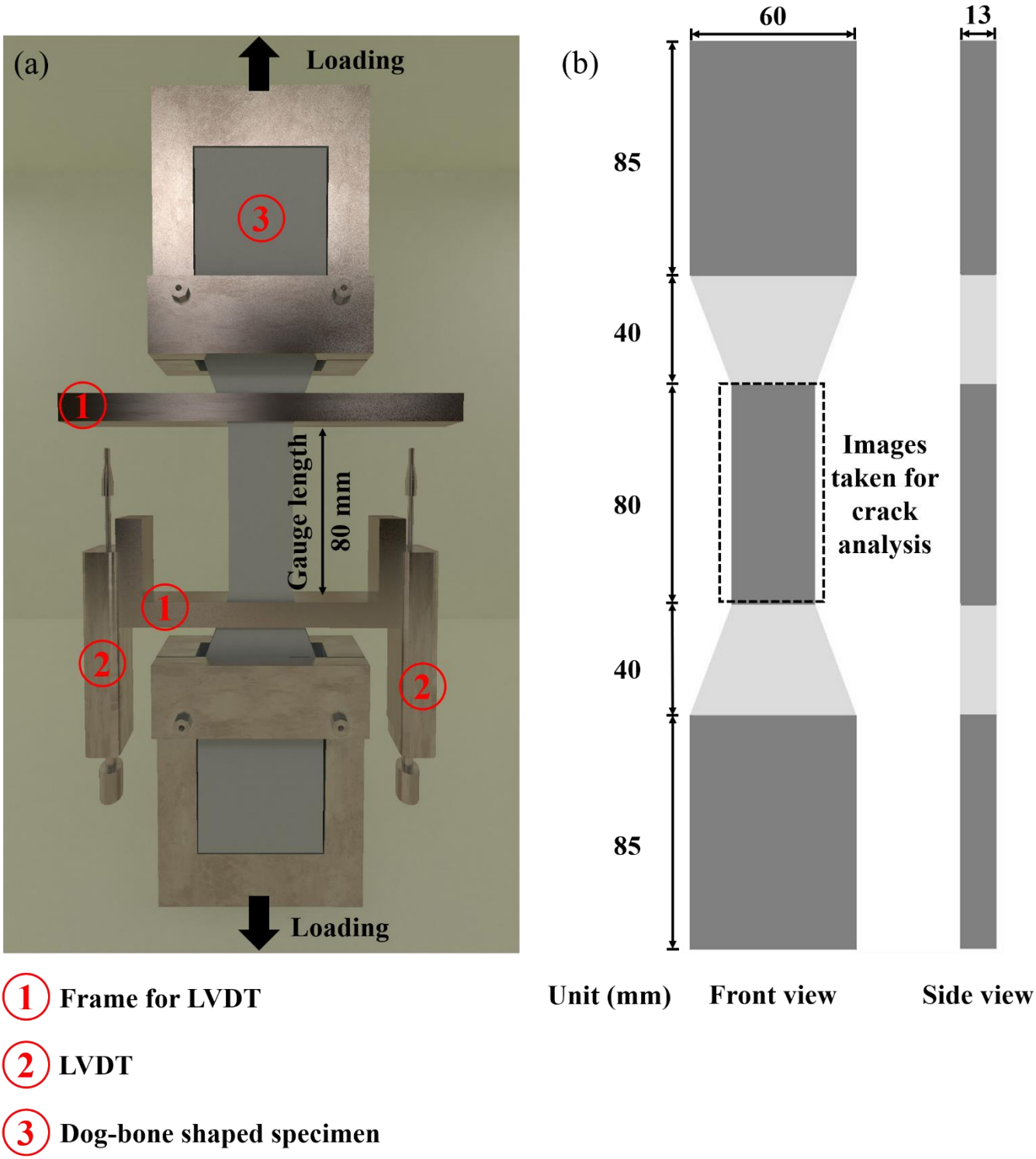

Fig. 5. Uniaxial direct tension test: (a) schematic illustration of the experimental setup; (b) dimension of the dog-bone shaped specimen.

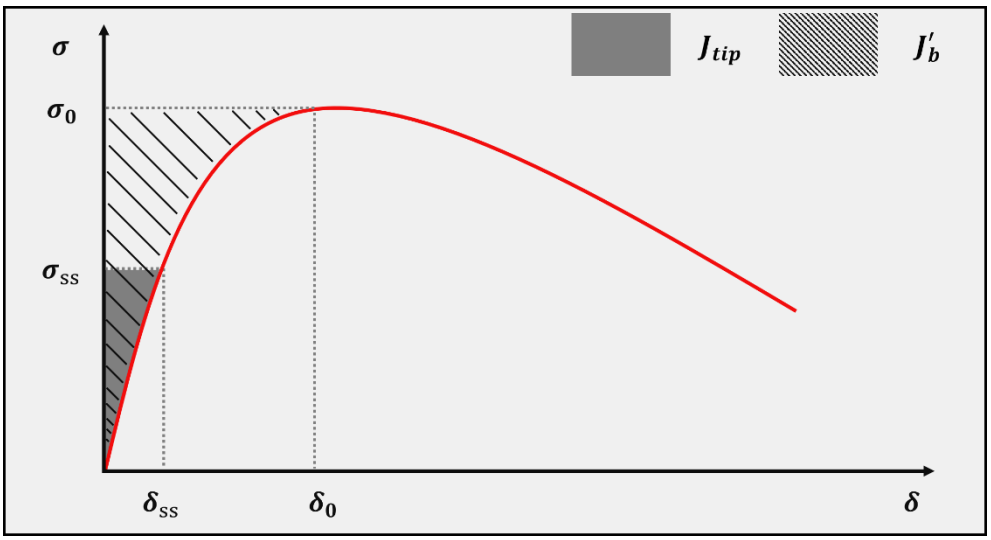

Fig. 6. Typical stress-crack opening curve for fibre bridging (modified from [1]).

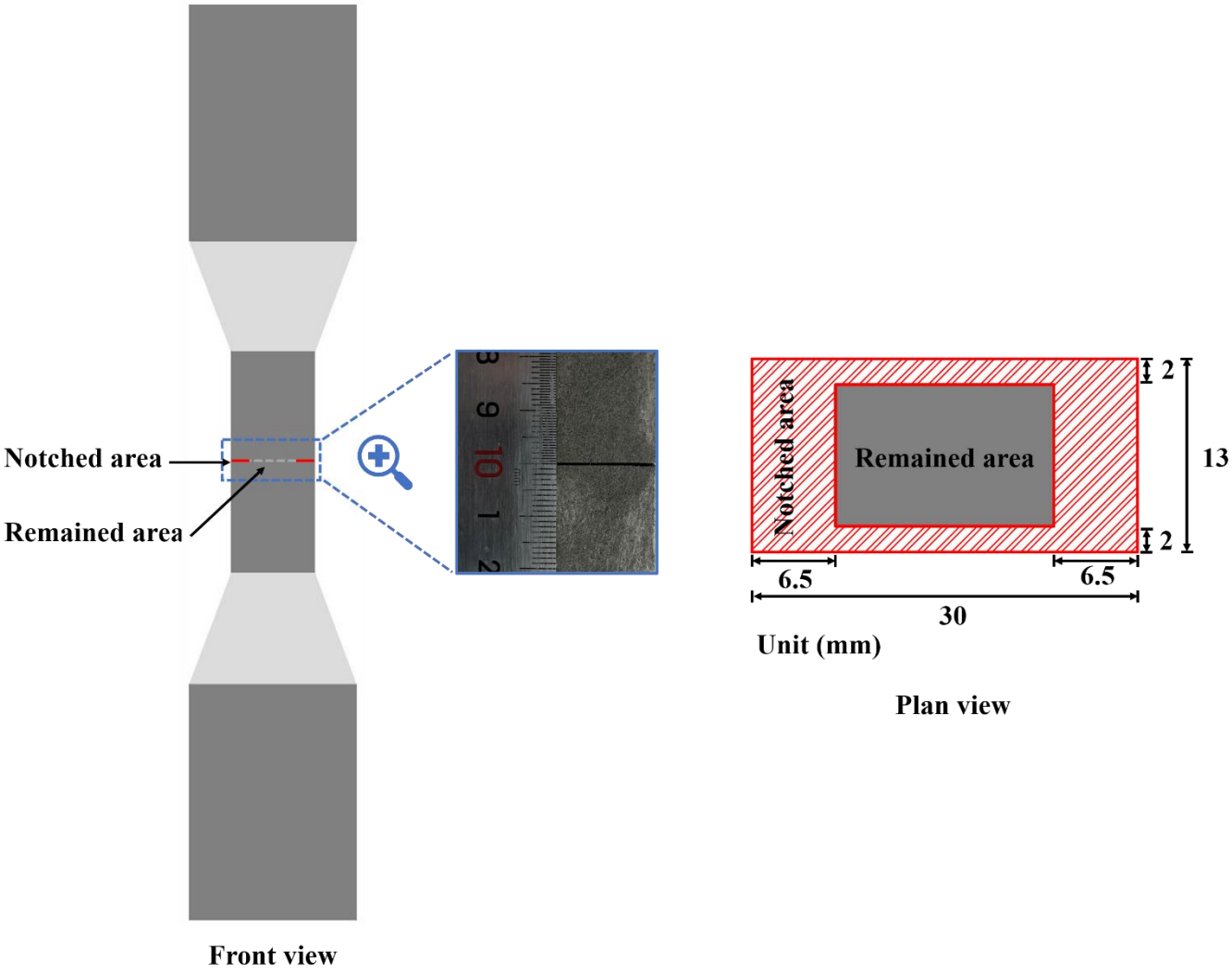

Fig. 7. Schematic illustration of the experimental configuration of single crack direct tension test.

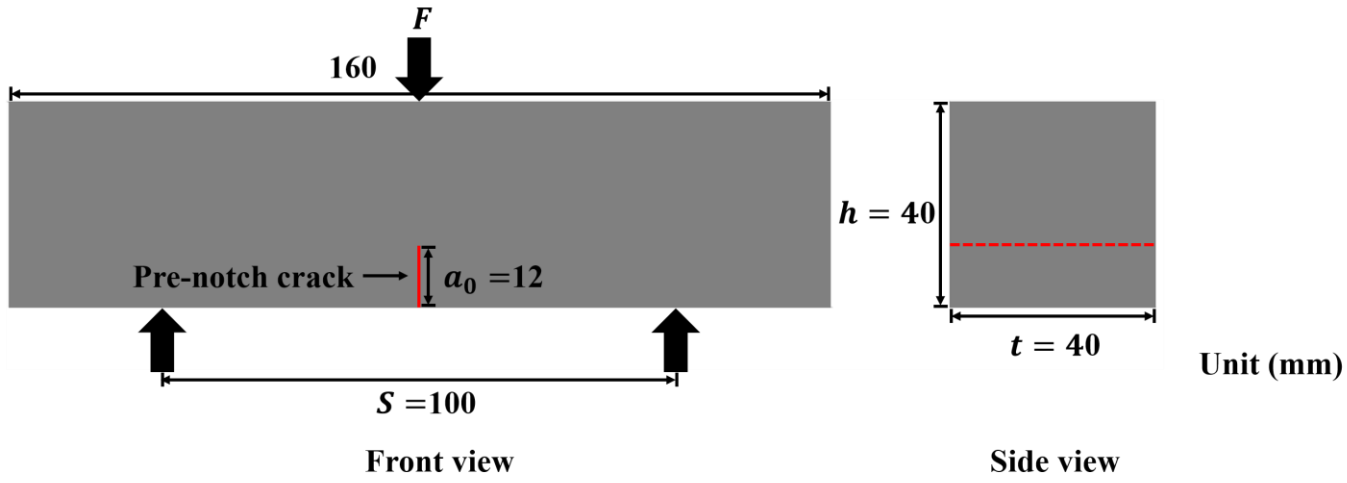

Fig. 8. Schematic illustration of three-point bending test for determining fracture toughness.

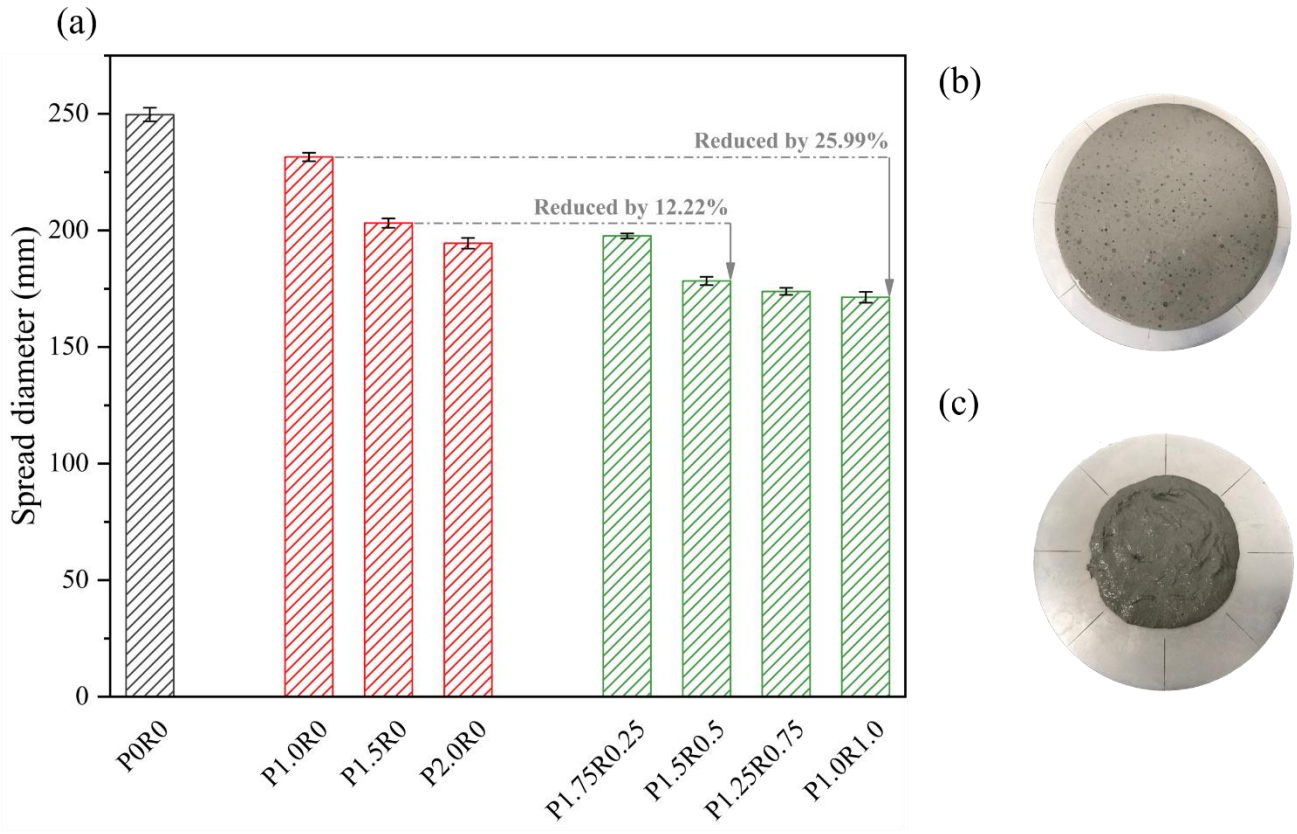

Fig. 9. (a) Effects of PVA and RTP fibres on flowability of SHGC; (b) Representative spread diameter picture of P0R0; (c) Representative spread diameter picture of P1.0R1.0.

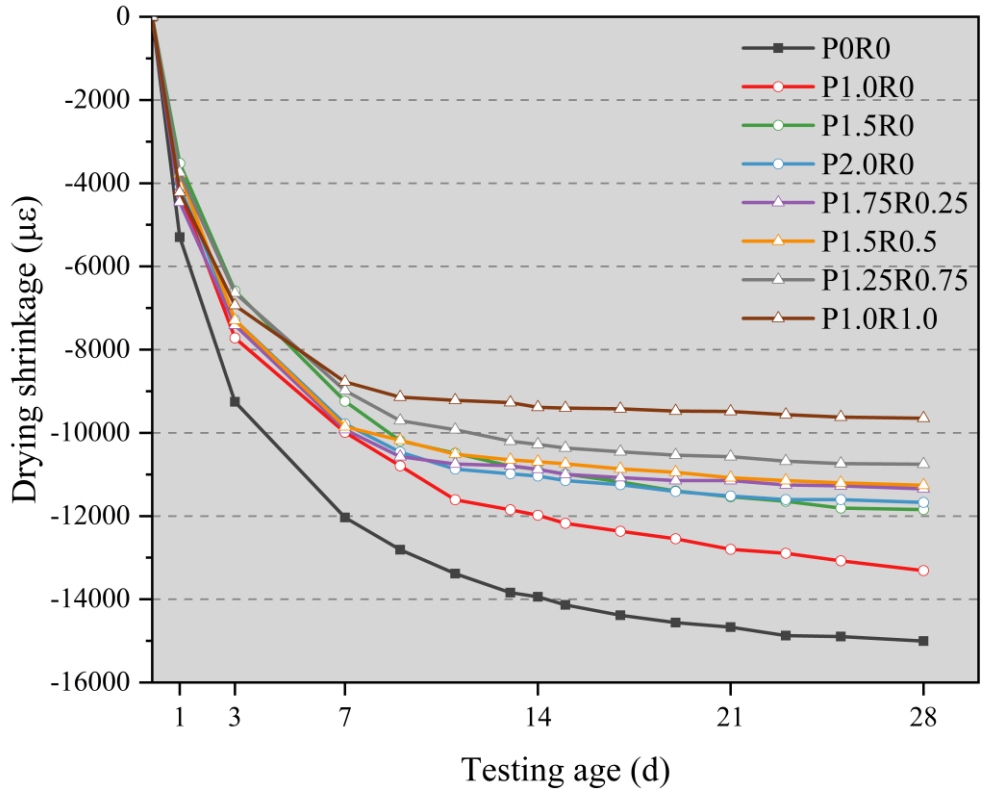

Fig. 10. Effects of PVA and RTP fibres on drying shrinkage of SHGC.

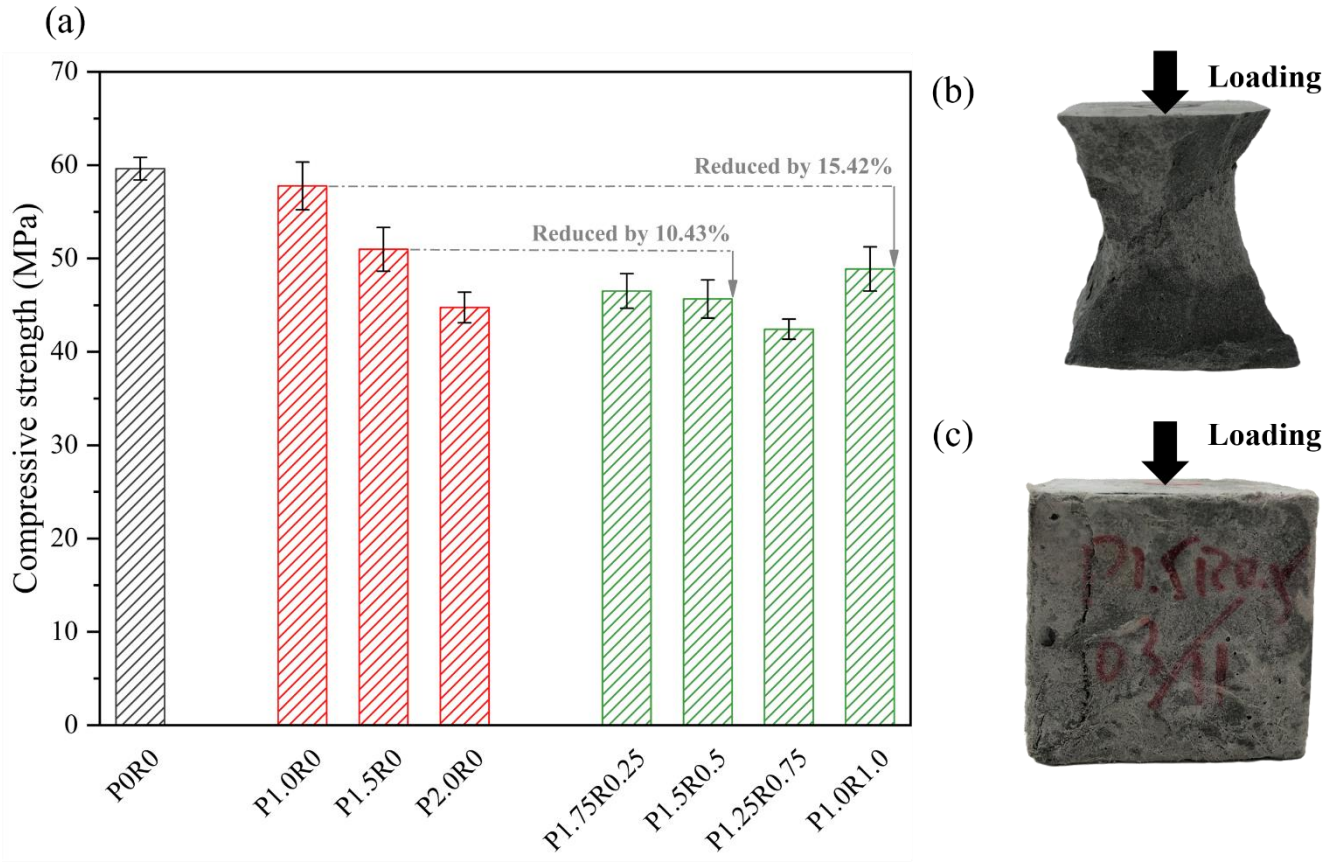

Fig. 11. (a) Effects of PVA and RTP fibres on 28-d compressive strength of SHGC; (b) Representative compressive failure pattern of P0R0; (c) Representative compressive failure pattern of P1.5R0.5.

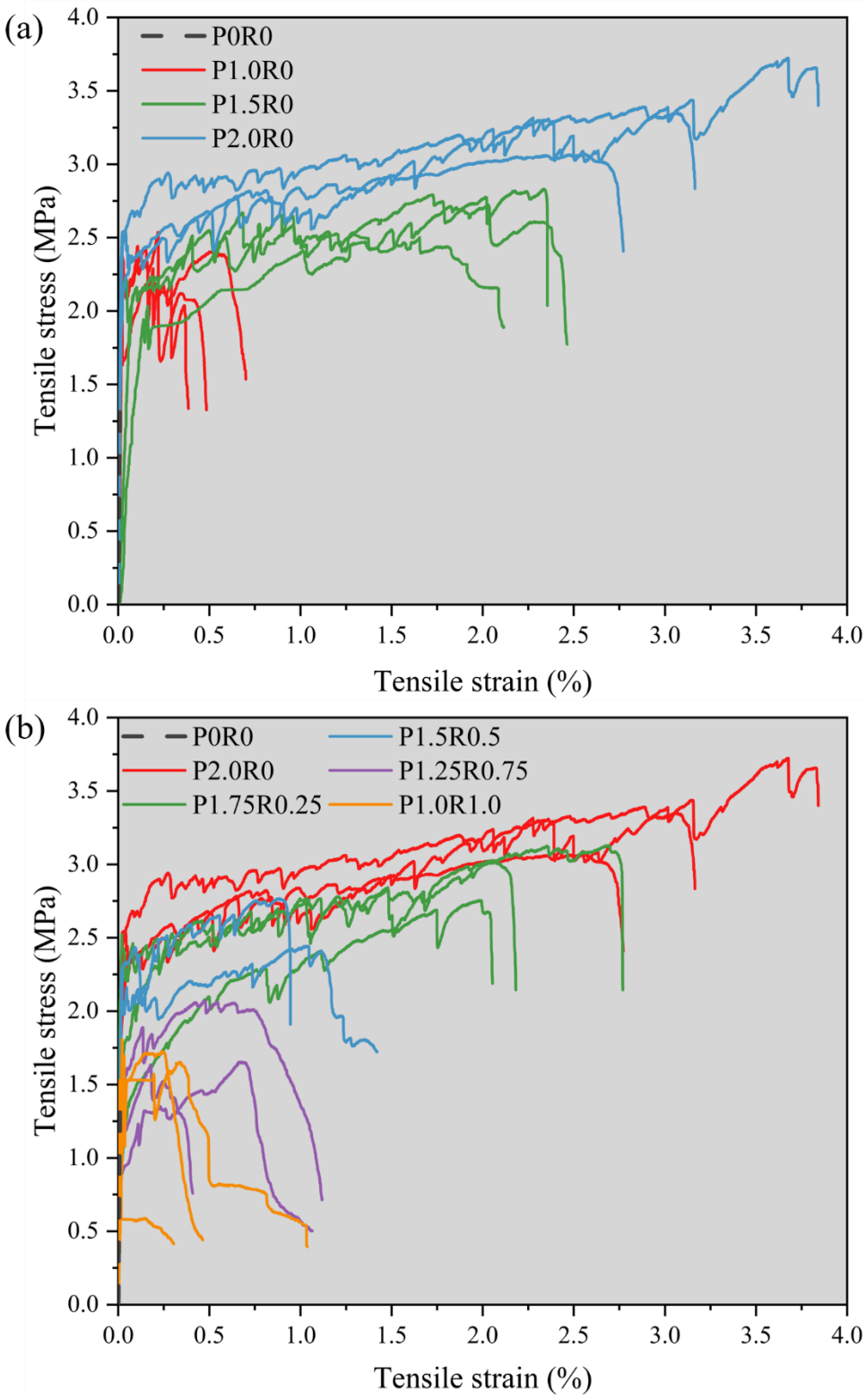

Fig. 12. Tensile stress-strain curves: (a) effect of PVA fibre; (b) effect of RTP fibre.

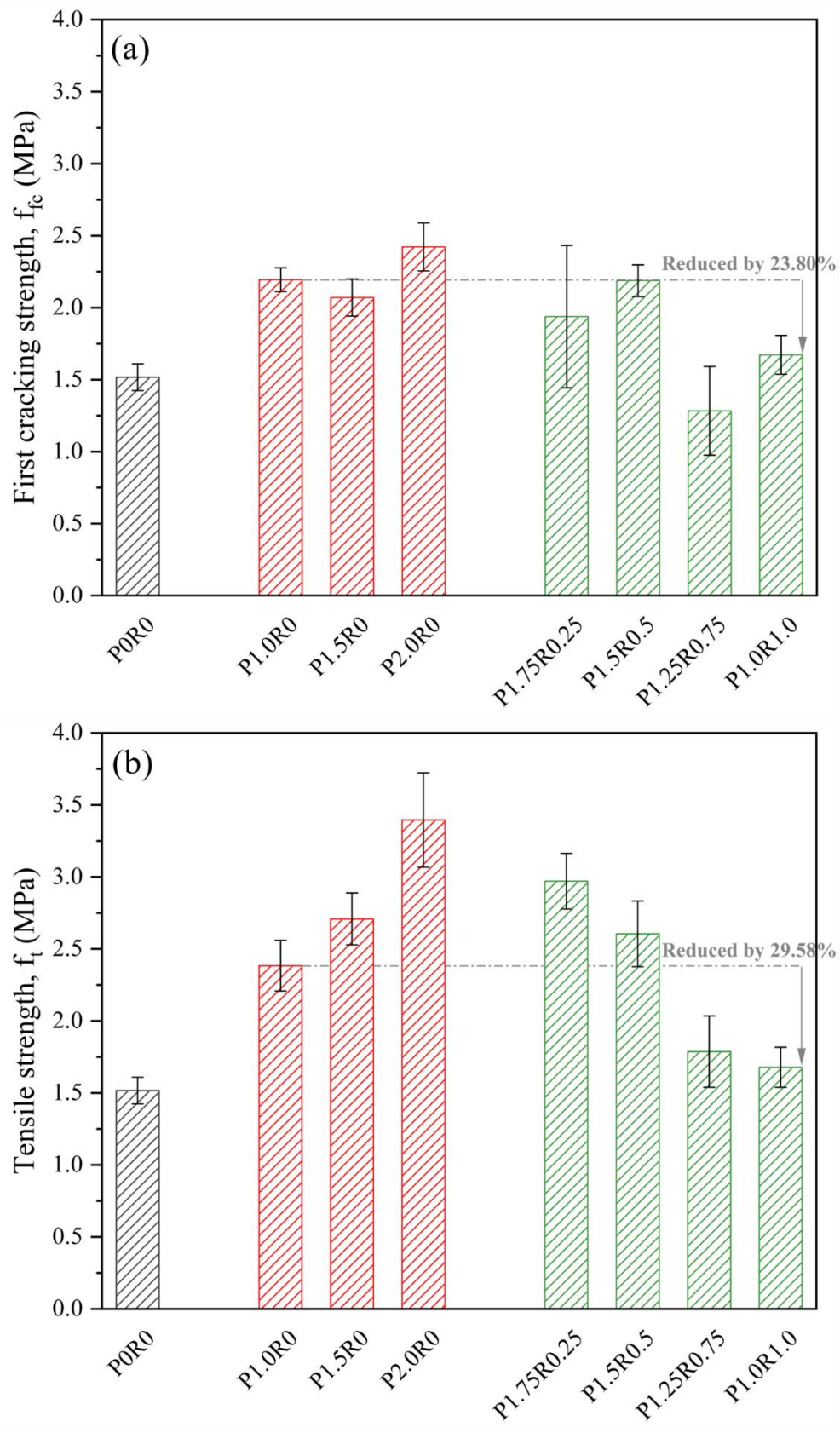

Fig. 13. (a) First cracking strength (f_{fc}) and (b) tensile strength (f_t) of all mixtures.

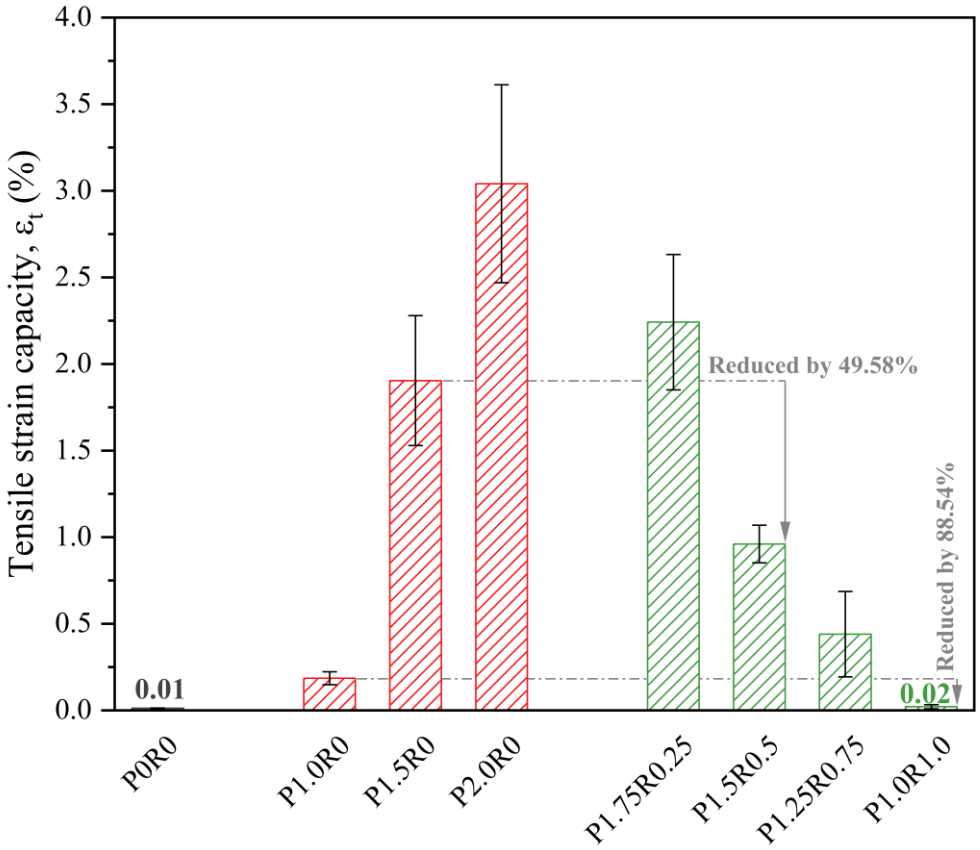

Fig. 14. Tensile strain capacity (ε_t) of all mixtures.

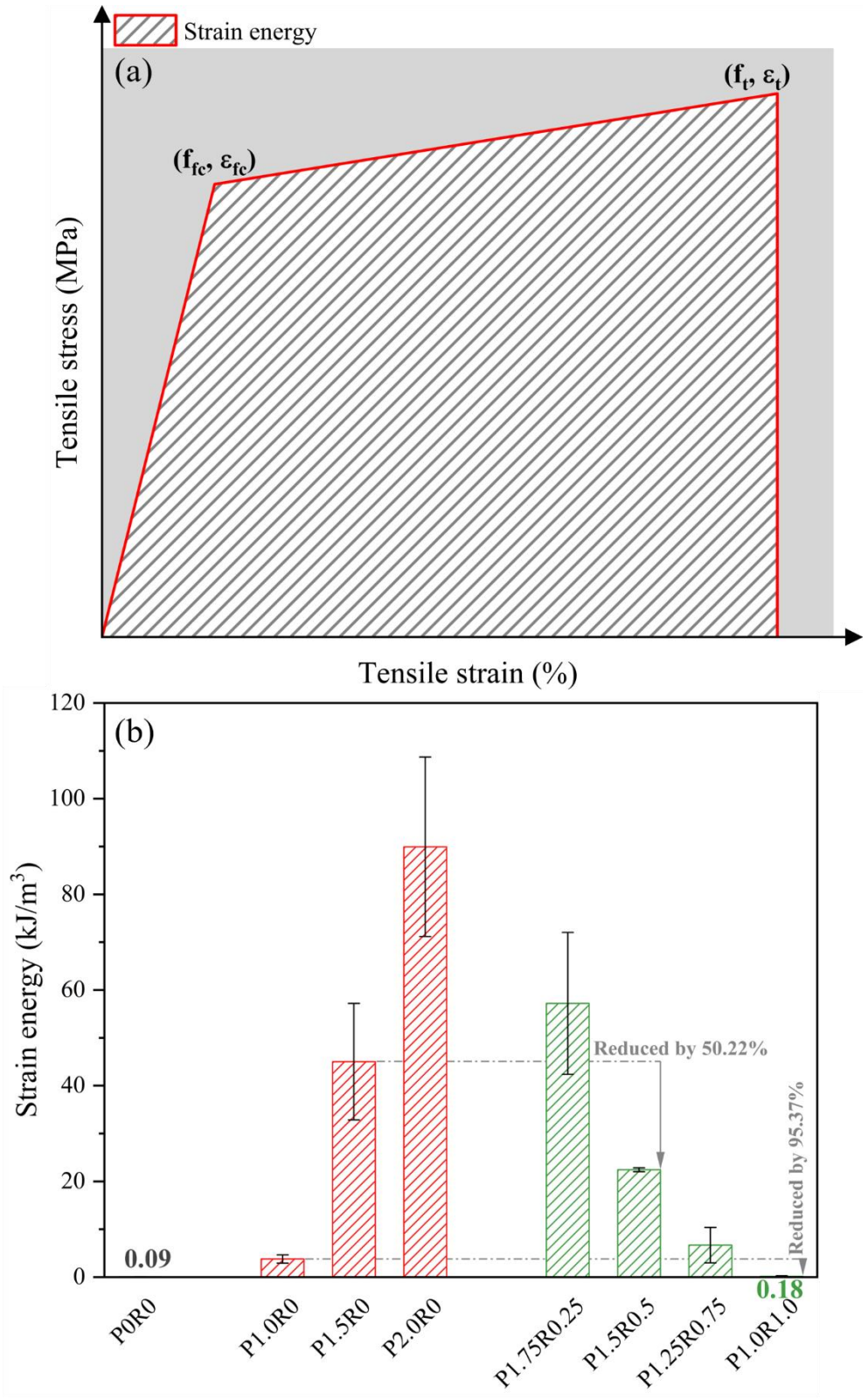

Fig. 15. (a) Schematic illustration of tensile strain energy; (b) tensile strain energy of all mixtures.

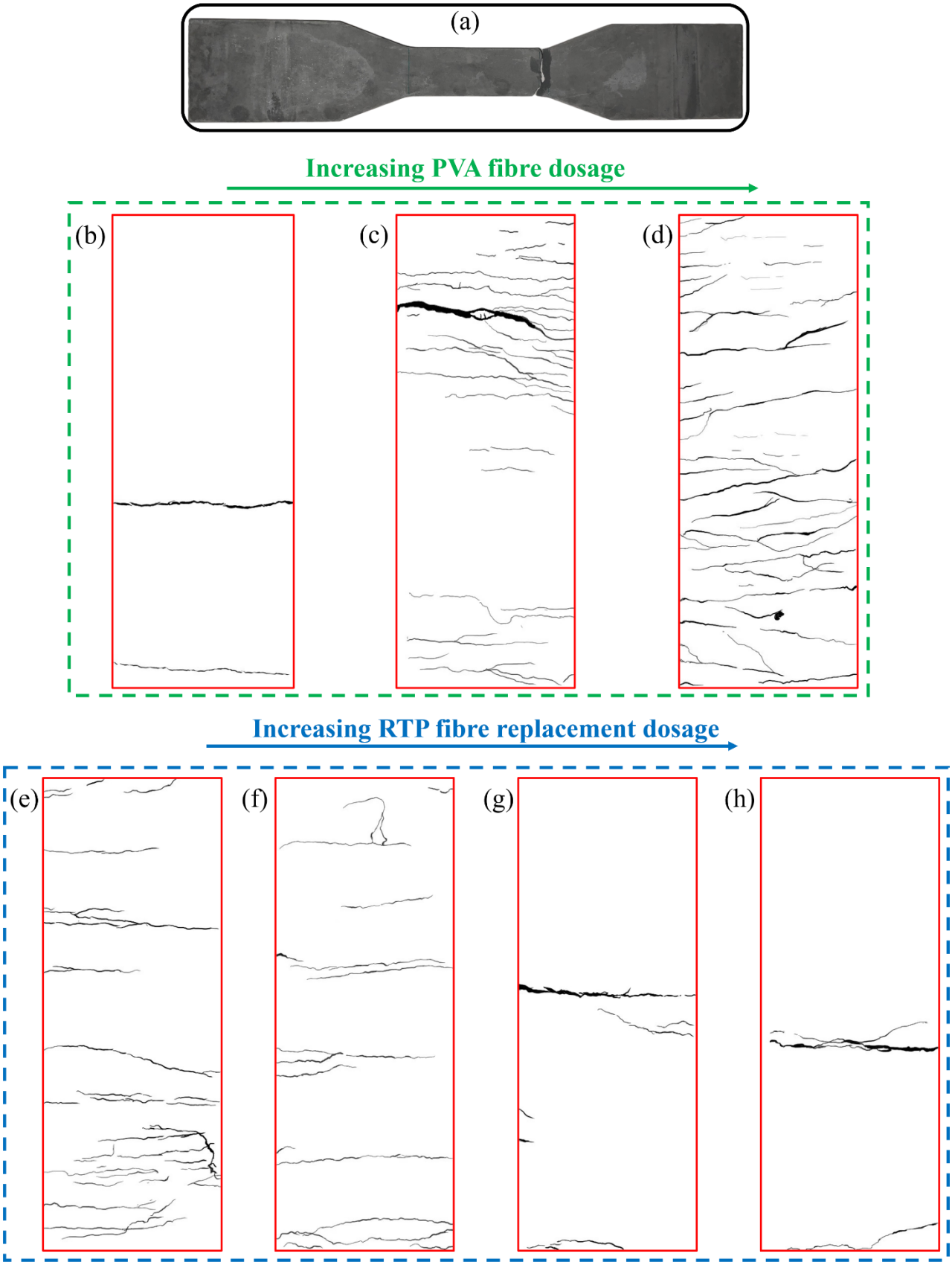

Fig. 16. Representative tensile cracking patterns of all mixtures: (a) P0R0; (b) P1.0R0; (c) P1.5R0; (d) P2.0R0; (e) P1.75R0.25; (f) P1.5R0.5; (g) P1.25R0.75; (h) P1.0R1.0.

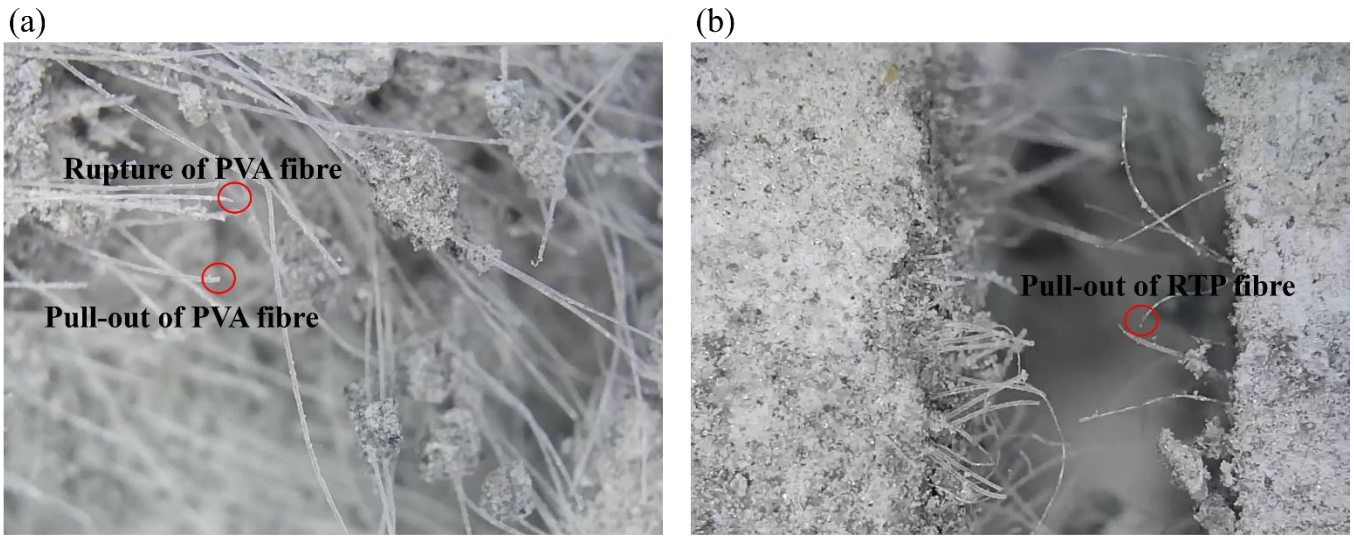

Fig. 17. Fibre conditions across the tensile fracture surfaces of SHGC: (a) Mono-PVA fibre reinforced SHGC; (b) Hybrid PVA and RTP fibre reinforced SHGC.

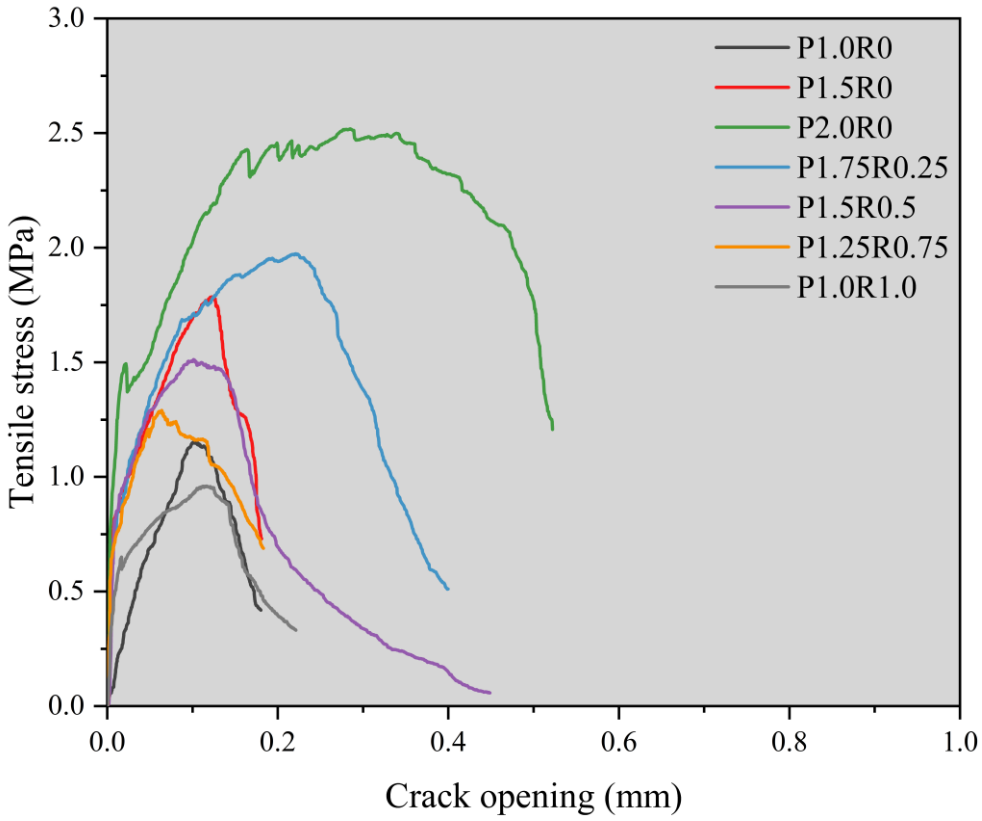

Fig. 18. Representative tensile stress-crack opening curves of SHGC.

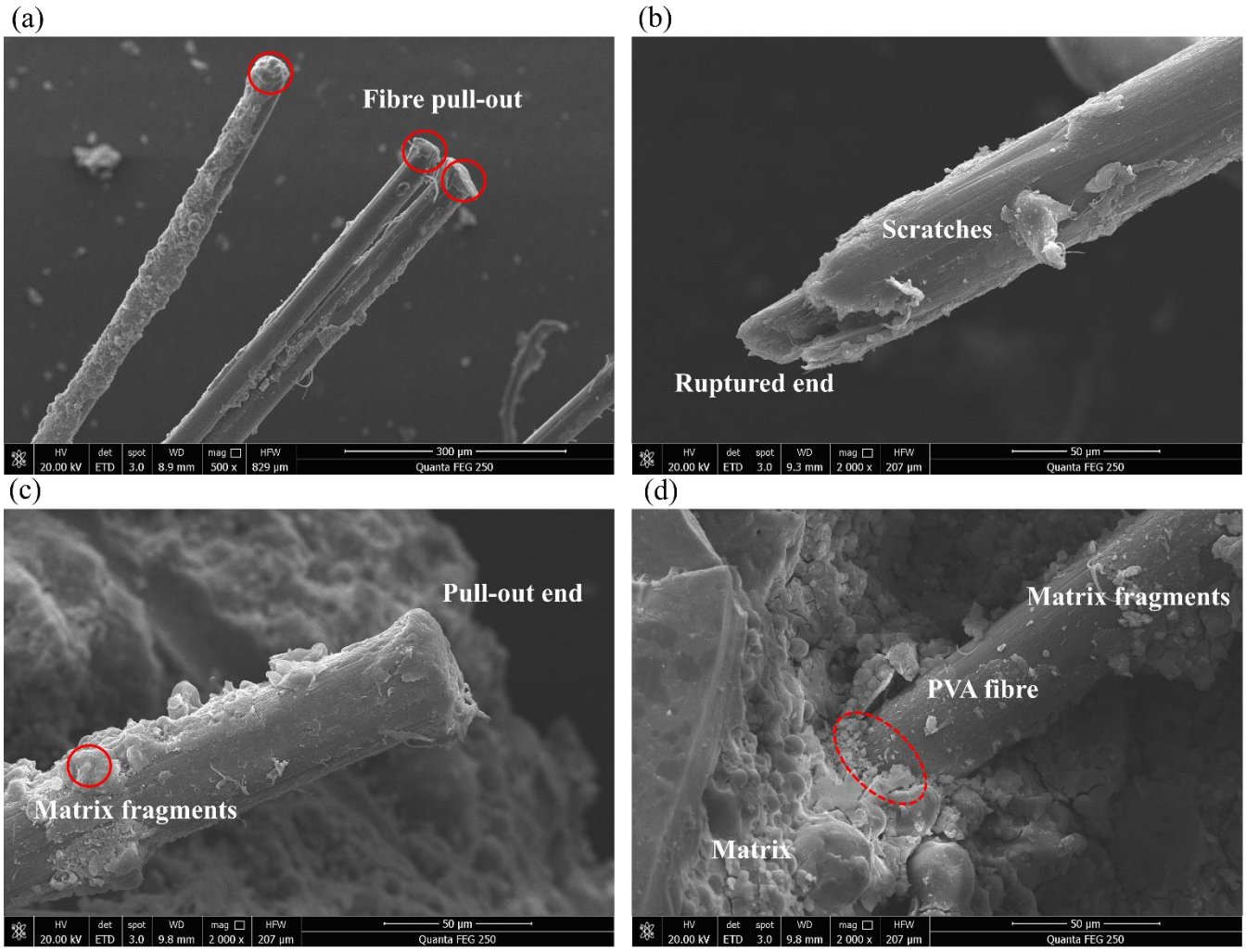

Fig. 19. SEM images of fibre morphology in mono-PVA fibre reinforced SHGC after uniaxial tensile failure.

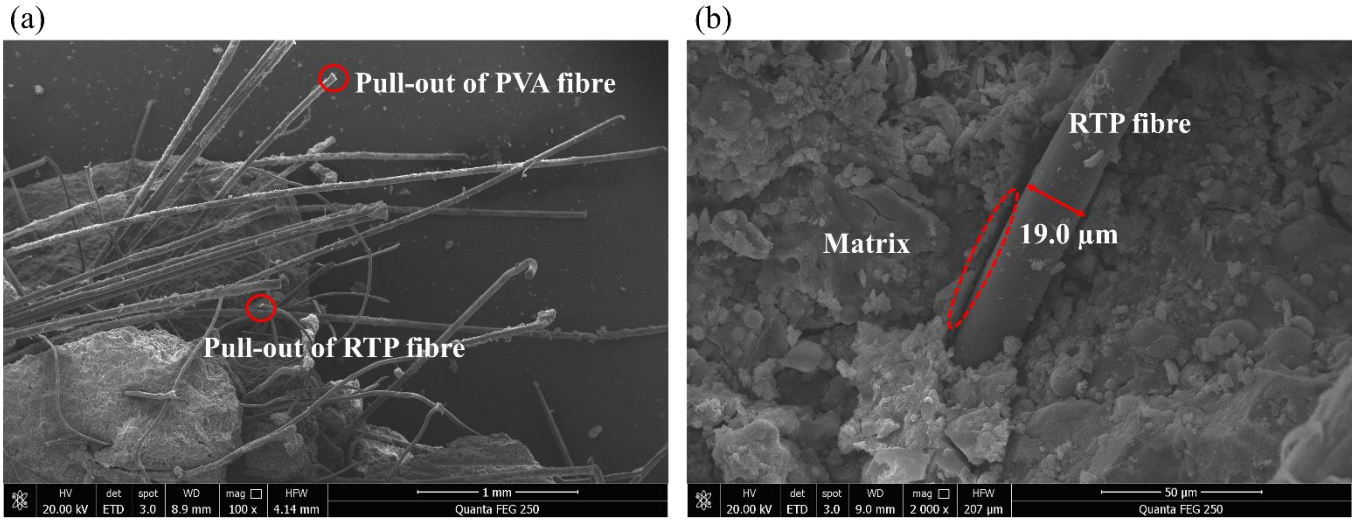

Fig. 20. SEM images of fibre morphology in hybrid PVA and RTP fibre reinforced SHGC after uniaxial tensile failure.

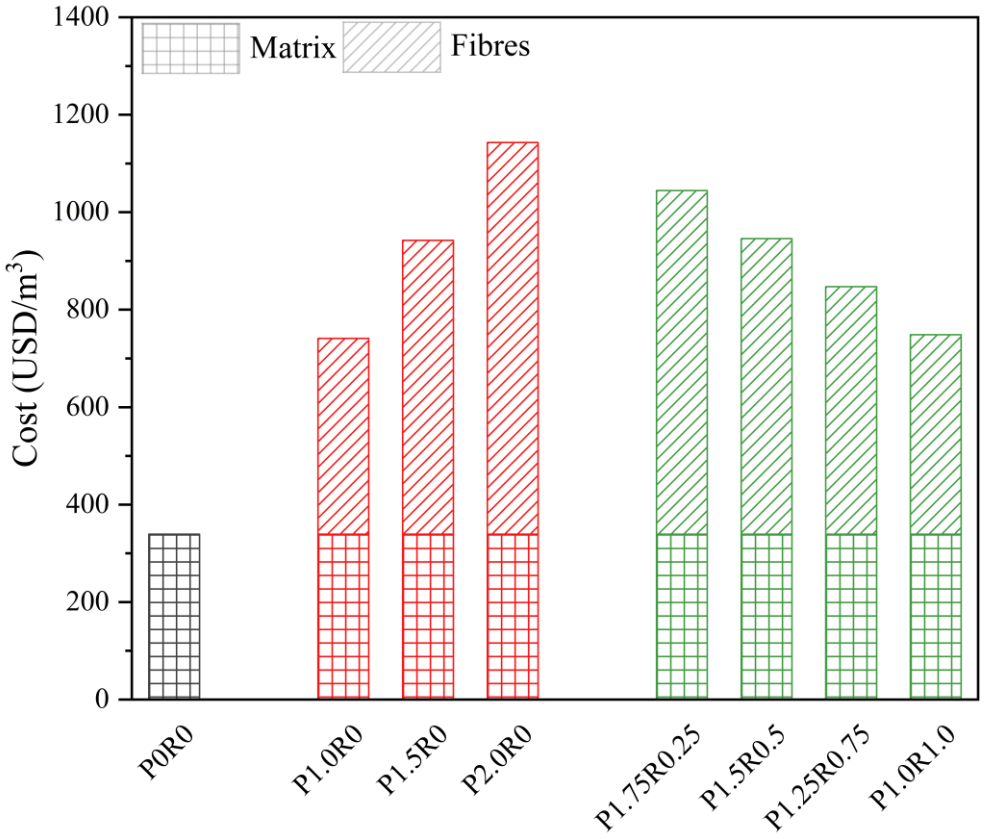

Fig. 21. Total material cost of all mixtures.

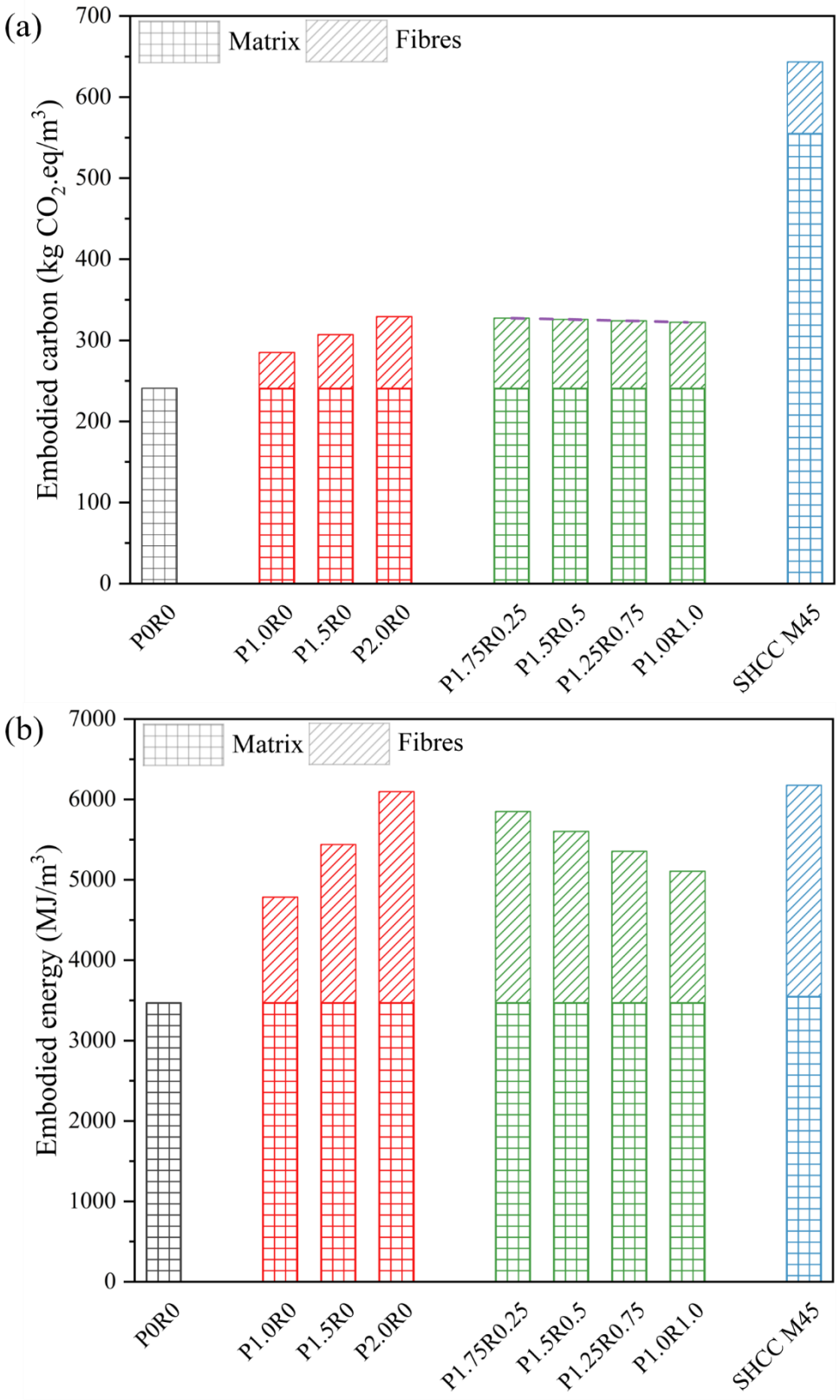

Fig. 22. (a) Embodied carbon and (b) embodied energy of all mixtures (note: SHCC M45 was used as comparison [99]).

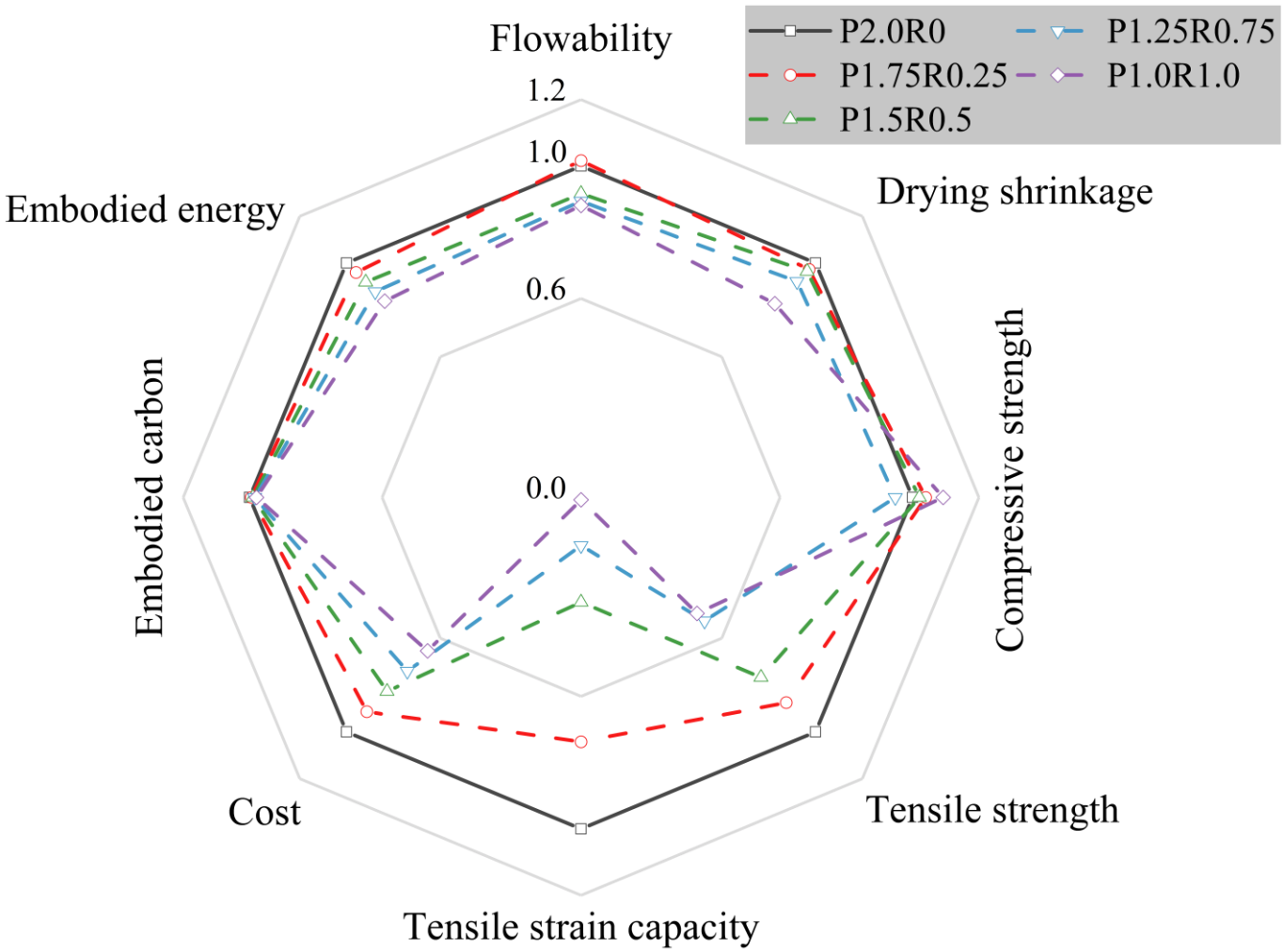

Fig. 23. Properties, economic and environmental comparison between mono-PVA fibre reinforced SHGC and hybrid fibre reinforced SHGC.

Table 1. Chemical composition and particle size of fly ash (FA) and ground granulated blast-furnace slag (GGBS).

	Oxide (wt%)									Average particle size (μm)
	SiO_2	Al_2O_3	Fe_2O_3	CaO	SO_3	MgO	TiO_2	P_2O_5	LOI	
FA	57.02	32.35	3.01	2.88	0.41	0.58	1.26	0.20	2.45	19.58
GGBS	31.85	17.31	0.34	41.20	1.78	6.13	0.62	0.02	0.39	9.78

Note: LOI (Loss on Ignition).

Table 2. Specific gravity of different ingredients (except fibres) in composites.

	FA	GGBS	Silica sand	SS	SH	SP
Specific gravity	2.19	2.90	2.66	1.38	1.31	1.06

Note: SS (sodium silicate); SH (sodium hydroxide); SP (superplasticiser).

Table 3. Properties of polyvinyl alcohol (PVA) fibre and recycled tyre polymer (RTP) fibre.

Properties/fibre type	PVA	RTP
Length (mm)	12.0	5.2 (2.4)
Diameter (μm)	40.0	21.4 (4.4)
Elongation at break (%)	6.5	20.6 (2.9)
Tensile strength (MPa)	1560	761 (115)
Elastic modulus (GPa)	41.0	3.8 (0.7)
Density (kg/m^3)	1300	1476 (3)

Note: the values are standard deviations in parentheses.

Table 4. Mix proportions of all mixtures in this study.

Mixture label	By weight					By volume (%)	
	Binder		Silica sand/binder	AL/binder	SP/binder	PVA fibre	RTP fibre
	FA	GGBS					
P0R0	0.8	0.2	0.2	0.45	0.01	0	0
P1.0R0						1.0	0
P1.5R0						1.5	0
P2.0R0						2.0	0
P1.75R0.25						1.75	0.25
P1.5R0.5						1.5	0.5
P1.25R0.75						1.25	0.75
P1.0R1.0						1.0	1.0

Note: AL (alkaline activator).

Table 5. Testing scheme of this study.

Type of test/mixture label		P0R0	P1.0R0	P1.5R0	P2.0R0	P1.75R0.25	P1.5R0.5	P1.25R0.75	P1.0R1.0
Flow table test	Number of specimens	3							
	Complied Standard	ASTM C1437-15 [62]							
Drying shrinkage test	Number of specimens	3							
	Complied Standard	ASTM C490-17 [63]							
Compression test	Number of specimens	4							
	Complied Standard	ASTM C109/C109M-20b [64]							
Uniaxial direct tension test	Number of specimens	3							
	Complied Standard	Recommendation of Japan Society of Civil Engineers [65]							
Single crack direct tension test	Number of specimens	-	3						
	Complied Standard	-	-						
Fracture toughness test	Number of specimens	4	-						
	Complied Standard	RILEM FMC-50 [68]	-						

Table 6. Residual crack number and crack width of SHGC after uniaxial direct tension test.

Mixture label	Average crack number	Average crack width (μm)
P1.0R0	4 (1)	218.9 (62.6)
P1.5R0	27 (15)	34.3 (7.5)
P2.0R0	28 (1)	29.8 (11.6)
P1.75R0.25	26 (2)	33.5 (2.2)
P1.5R0.5	17 (2)	39.2 (0.2)
P1.25R0.75	8 (6)	124.7 (75.4)
P1.0R1.0	3 (1)	379.9 (190.0)

Note: the values are standard deviations in parentheses.

Table 7. Results of single crack direct tension test.

Mixture label	Fibre bridging stress, σ_0 (MPa)	Corresponding crack opening, δ_0 (mm)
P1.0R0	1.20 (0.157)	0.114 (0.014)
P1.5R0	1.91 (0.126)	0.157 (0.048)
P2.0R0	2.56 (0.130)	0.308 (0.030)
P1.75R0.25	2.02 (0.172)	0.218 (0.030)
P1.5R0.5	1.64 (0.161)	0.112 (0.036)
P1.25R0.75	1.51 (0.155)	0.083 (0.032)
P1.0R1.0	1.08 (0.140)	0.140 (0.048)

Note: the values are standard deviations in parentheses.

Table 8. Fracture toughness of geopolymer matrix (P0R0).

Specimen	Mass, m (kg)	Peak load, F_p (kN)	Fracture toughness, K_m (MPa·m$^{1/2}$)
1	0.489	0.112	0.572
2	0.481	0.123	0.628
3	0.492	0.110	0.562
4	0.482	0.094	0.480
Average			0.560 (0.061)

Note: the values are standard deviations in parentheses.

Table 9. Calculated strain hardening indices of SHGC.

Mixture label	Strength criterion		Energy criterion		
	σ_{fc} (MPa)	σ_0/σ_{fc}	J_{tip} (J/m^2)	J_b' (J/m^2)	J_b'/J_{tip}
P1.0R0		0.79 (0.104)		56.78	2.34 (0.836)
P1.5R0		1.26 (0.083)		75.91	3.13 (0.697)
P2.0R0		1.69 (0.086)		139.21	5.75 (2.534)
P1.75R0.25	1.52	1.33 (0.114)	24.22	93.55	3.86 (1.136)
P1.5R0.5		1.08 (0.106)		47.30	1.95 (0.994)
P1.25R0.75		1.00 (0.102)		37.51	1.55 (1.211)
P1.0R1.0		0.71 (0.092)		38.25	1.58 (0.905)

Note: the values are standard deviations in parentheses.

Table 10. Cost and life cycle inventory data of all components in SHGC.

Type	Cost (USD/kg)	Embodied carbon (kg CO_2.eq/kg)	Embodied energy (MJ/kg)
FA [90, 93]	0.0363	0.01	0.1
GGBS [91, 93]	0.0678	0.07	1.33
Silica sand [92, 94]	0.0250	0.025	0.17
SH [11, 90]	1.03	0.86	18
SS [90, 95]	0.64	0.43	4.6
Water	0.001	0	0
SP [92, 94, 97]	1.21	1.5	35
PVA fibre [96]	30.92	3.4	101
RTP fibre [93]	0.5	2.53	21.9